IMPROVEMENT OF FOURIER TRANSFORM ION CYCLOTRON RESONANCE

MASS SPECTROMETRY DETECTION TECHNOLOGY

By

CHAD RANDAL WEISBROD M.S.

A thesis submitted in partial fulfillment of
the requirements for the degree of

MASTER OF SCIENCES IN CHEMISTRY

WASHINGTON STATE UNIVERSITY
Department of Chemistry

MAY 2010

To the Faculty of Washington State University:

The members of the Committee appointed to examine the thesis of Chad Randal Weisbrod find it satisfactory and recommend that it be accepted.

James E. Bruce, Ph.D., Chair

Kenneth L. Nash, Ph.D.

Herbert H. Hill, Ph. D.

William Siems, Ph.D.

Acknowledgments

First and foremost, I want to thank my family for love and support.

I would like to thank everyone involved in shaping me into the scientist I have become. Many have been pivotal in this process and deserve mention, however, I will inevitably miss someone (this is not intentional). I would like to thank Robin S. Tanke for taking me under her wing as an undergraduate and making me understand the importance behind doing fundamental research in chemistry. It was in her laboratory that I first acquired experience and desire for research. Without her guiding influence in my life I am certain I would not have been able to complete this work. The faculty of the University of Wisconsin Stevens Point (UWSP) chemistry department provided an unparalleled academic environment with the resources available. I would like to thank the faculty of UWSP for their dedication to scientific education.

I would like to thank my colleagues Gunnar E. Skulason and Nathan K. Kaiser for being the best possible people to work with. They both had the uncanny ability to teach me something new every day I spent with them (most days more than just one new something). With the collaborative efforts of both of these individuals, I was able to complete the research described herein. Nathan specifically imbued the concept of hard work and diligence comes with great reward. In addition, he showed me early in my graduate career that anything can be accomplished. Gunnar never ceased to amaze me with the width and breadth of his knowledge. He taught me most of what I presently understand about electronics and circuit boards.

Last, but certainly not least I would like to thank my advisor James E. Bruce for his immeasurable contribution to this project and his molding me into an effective scientist. Jim's willingness to teach me the art of instrumentation is what really kept me engaged early in my graduate career. The skills I have learned and continue to learn in Jim's laboratory will serve me for the rest of my life. As Jim's student I witnessed his dedicated to providing the best possible learning experience for all in the laboratory. He

typifies what a good mentor should be: approachable, excited about science, and willing to embrace the ideas of his students. I hope that one day I can make the same mark upon others lives that he has upon mine.

Improvement of Fourier Transform Ion Cyclotron Resonance

Mass Spectrometry Detection Technology

Abstract

By Chad R. Weisbrod M.S

Washington State University

May 2010

Chair: James E. Bruce

Described herein are two novel FTICR-MS cells designed to increase performance: Trapping Ring Electrode Cell (TREC) and excite-coupled Trapping Ring Electrode Cell(eTREC). TREC permits the ability to maintain coherent ion motion at larger initial excited cyclotron radii by decreasing the change in radial electric field with respect to *z*-axis position in the cell. Resolving power approaching the theoretical limit was achieved using the novel TREC technology; over 420,000 resolving power was observed on melittin $[M+4H]^{4+}$ species when employed under modest magnetic field strength (3T). A tenfold gain in signal-to-noise ratio (S/N) is demonstrated over the closed cylindrical cell optimized with common potentials on all ring electrodes. The observed frequency drift during signal acquisition over long time periods was also significantly reduced, resulting in improved resolving power. eTREC technology provides greater linearity in the excitation electric field along with minimized variation in radial trapping field during detection. Using this technology sensitivity was increased by >50%, resolution of $^{13}C_2$ and ^{34}S fine structure peaks was achieved with the peptide MMMMG (~330,000 RP) on a 3 Tesla system, and the limit of detection was significantly reduced.

Table of Contents

List of Figures

Chapter I: Introduction to FTICR-MS

The Fourier Transform Ion Cyclotron Resonance Mass Spectrometer (FTICR-MS) was first introduced by Marshall and Commisorrow in 1974[1]. Since its introduction, FTICR-MS was demonstrated to posses attributes such as incredibly high resolving power, mass measurement accuracy, sensitivity, and dynamic range. The technique has flourished since its inception and is now widely utilized[2-4]. FTICR-MS is often called upon for mass measurement of extraordinarily complex mixtures such as are found in the fields of proteomics, petroleomics, and metabolomics. In addition, physicists have employed FTICR-MS and close derivatives in the study of fundamental particles[5]. The study of in-tact proteins, commonly called top-down proteomics[6-8], would not exist without FTICR-MS. A close relative of FTICR-MS, the Orbitrap[9], borrows many of its principles of operation from that of its more established counterpart.

A typical FTICR-MS experiment consists of three basic steps: ion accumulation, ion transfer, and mass analysis. The ion accumulation phase of an experiment is usually conducted within the instrument near the source region at relatively high pressure[10]. A multi-pole storage device is utilized to accumulate and thermalize ions external to the magnetic field. In modern FTICR-MS instruments, some type of mass selection or mass analysis occurs prior to transfer to the ICR cell[11]. This mass analysis is performed prior to (as in the Bruker Apex Q) or during ion accumulation (as in the LTQ-FT). Subsequently, the accumulated population of ions is transmitted to the ICR cell via multi-pole ion guides or ion optics. Finally, ions are sampled from the cloud approaching the cell by lowering the DC potential applied to the entry plate of the cell, waiting for the ions to enter, and raising this plate voltage to trap the ions. Once confined the m/z of the ions are analyzed.

Many principals need to be considered to understand how the FTICR-MS cell accomplishes mass analysis. The FT-ICR mass spectrometer relies upon an electromagnetic ion trap or cell to confine ions during detection[12-14]. The confinement is accomplished radially (*x*-*y* dimension) by an applied magnetic field parallel to the *z*-axis of the ion trap. Axial ion confinement is performed using DC electrical

potentials applied to trapping electrodes. As an ion approaches either trap plate, it experiences a force due to the applied electrostatic electric field, and its kinetic energy is converted to potential energy. Thus, the ion exhibits periodic motion similar to the classical harmonic oscillator. As a consequence of the method by which ions are trapped within the cell, four natural motions arise. Trapping oscillation is the motion in which the ions oscillate in the z-dimension of the cell. Cyclotron motion is caused by the Lorentz force and is dependent upon the mass-to-charge ratio (*m*/*z*) (Equation 1).

$$\omega_c = \frac{qB_o}{m} = \frac{zeB_o}{m} \qquad (1)$$

Where ω_c is the cyclotron frequency, *z* is number of charges, *e* is the charge of an electron, B_o is the magnetic field strength, and *m* is the mass. Equation 1 represents the unperturbed cyclotron frequency, which is only dependent upon the *m*/*z* of the ion and the magnetic field strength. The third motion, magnetron motion, is caused by the outward directed radial component of the electrostatic field confining the ions in finite FT-ICR cells[15]. The radial electric field is perpendicular to the magnetic field and results in the $\vec{E} \times \vec{B}$ drift of the ions around the center of the ICR cell. Ion cloud rotation, the final of the four natural motions, results from the electric field generated by the ion cloud itself[16].

Signal duration, and consequently performance, in FTICR-MS is influenced by many factors, but the two most notable contributors to decreased signal duration are collisional damping[17] and ion-cloud dephasing[16]. Collisional damping is a signal decay process which is proportional to pressure; therefore, reducing the pressure in the cell region decreases signal decay, due to fewer collisions. The coherent motion of ions of a given *m*/*z* after initial excitation to some cyclotron orbit will induce an image current on the detection electrodes. As ions become increasingly out of phase, the image current decreases in magnitude and is lost when equal numbers of ions of the same *m*/*z* are 180^o out of phase in their cyclotron orbit. This dephasing process is thought to be caused by a culmination of effects. The three which have been documented: magnetic field inhomogeneity, electric field inhomogeneity[18-20], and

Coulombic interactions[21-24] occurring between ion clouds of differing *m*/*z*. Additionally, the applied electrical potentials in the trapping region of the cell result in a component of the electric field acting upon the ions radially. This radially outward directed force is one of the major mechanisms thought to be responsible for ion cloud dephasing (magnetron motion)[25-27]. Many high resolution FT-ICR measurements employ relatively low trapping potentials in order to minimize electric field inhomogeneity and its deleterious effect on coherent ion motion[28, 29]. The use of low trapping potentials requires that the ions entering the cell have sufficiently low kinetic energy to remain confined. Collisional cooling is a method of thermalizing ion kinetic energy; however, the undesirable pump-down time required to regain the low pressure needed for measurement ($\leq 10^{-9}$ torr) hinders high-throughput analysis. Magnetron frequency and space charge normally both reduce the observed cyclotron frequency as illustrated in Equation 2[30].

$$\omega_{obs.} = \omega_c - \omega_m - \delta \qquad (2)$$

In Equation 2, $\omega_{obs.}$, ω_c, ω_m, δ are the observed cyclotron frequency, the "unperturbed" cyclotron frequency, the magnetron frequency, and the collective effect of ion-ion interactions, respectively. It should be noted that the sign of the magnetron frequency term is dependent upon the direction of the radial component of the electric field force acting on an ion[31]. Outward-directed radial fields result in magnetron motion opposed to cyclotron motion, and thus, reduce the observed cyclotron frequency.

Maintaining coherent motion of the ion cloud within the ion trap is crucial to signal intensity and duration in an FT-ICR experiment[32], since the image current induced by the coherent ion packet diminishes as dephasing occurs. Thus, minimizing dephasing mechanisms can increase instrument performance. A previous investigation by our laboratory demonstrated that reducing the outward directed force, which arises from the application of trapping potentials, has a favorable effect in that observed cyclotron frequency was shown to be independent of ion position along the *z*-axis within the

cell[33]. Differences in reduced cyclotron frequency among ions (of the same m/z) with coherent cyclotron motion eventually leads to ion cloud dephasing and the decay of ICR signal with time.

(1) Comisarow, M. B.; Marshall, A. G. *Chemical Physics Letters* 1974, *25*, 282-283.

(2) Schmid, A.; Gehlenborg, N.; Bodenmiller, B.; Mueller, L. N.; Campbell, D.; Mueller, M.; Aebersold, R.; Domon, B. *Molecular and Cellular Proteomics* 2008, *7*, 2138-2150.

(3) Tolmachev, A. V.; Monroe, M. E.; Purvine, S. O.; Moore, R. J.; Jaitly, N.; Adkins, J. N.; Anderson, G. A.; Smith, R. D. *Analytical Chemistry (Washington, DC, United States)* 2008, *80*, 8514-8525.

(4) Wenger, C. D.; Boyne, M. T.; Ferguson, J. T.; Robinson, D. E.; Kelleher, N. L. *Analytical Chemistry (Washington, DC, United States)* 2008, *80*, 8055-8063.

(5) Bergstroem, I.; Nagy, S.; Schuch, R.; Blaum, K.; Fritioff, T. *Springer Proceedings in Physics* 2004, *92*, 397-418.

(6) Ferguson, J. T.; Wenger, C. D.; Metcalf, W. W.; Kelleher, N. L. *Journal of the American Society for Mass Spectrometry* 2009, *20*, 1743-1750.

(7) Tolmachev, A. V.; Robinson, E. W.; Wu, S.; Pasa-Tolic, L.; Smith, R. D. *International Journal of Mass Spectrometry* 2009, *287*, 32-38.

(8) Vellaichamy, A.; Tran, J. C.; Catherman, A. D.; Lee, J. E.; Kellie, J. F.; Sweet, S. M. M.; Zamdborg, L.; Thomas, P. M.; Ahlf, D. R.; Durbin, K. R.; Valaskovic, G. A.; Kelleher, N. L. *Analytical Chemistry (Washington, DC, United States)*, *82*, 1234-1244.

(9) Hu, Q.; Noll, R. J.; Li, H.; Makarov, A.; Hardman, M.; Cooks, R. G. *Journal of Mass Spectrometry* 2005, *40*, 430-443.

(10) Senko, M. W.; Hendrickson, c. L.; Emmett, M. R.; Shi, S. D. H.; Marshall, A. G. *Journal of the American Society for Mass Spectrometry* 1997, *8*, 970-976.

(11) Syka, J. E. P.; Marto, J. A.; Bai, D. L.; Horning, S.; Senko, M. W.; Schwartz, J. C.; Ueberheide, B.; Garcia, B.; Busby, S.; Muratore, T.; Shabanowitz, J.; Hunt, D. F. *Journal of Proteome Research* 2004, *3*, 621-626.

(12) Dehmelt, H. *Reviews of Modern Physics* 1990, *62*, 525-530.

(13) McIver, R. T., Jr. *Review of Scientific Instruments* 1970, *41*, 555-558.

(14) Penning, F. M. *Nederlands Tijdschrift voor Natuurkunde (1934-1976)* 1936, *3*, 141-154.

(15) Marshall, A. G.; Guan, S. *Phys. Scr. T* 1995, *T59*, 155-164.

(16) Peurrung, A. J.; Kouzes, R. T. *Physical Review E: Statistical Physics, Plasmas, Fluids, and Related Interdisciplinary Topics* 1994, *49*, 4362-4368.

(17) Marshall, A. G.; Comisarow, M. B.; Parisod, G. *Journal of Chemical Physics* 1979, *71*, 4434-4444.

(18) Mitchell, D. W.; Hearn, B. A.; DeLong, S. E. *International Journal of Mass Spectrometry and Ion Processes* 1993, *125*, 95-126.

(19) Capron, M. A.; Haskin, S. S.; Hanson, C. D. *Journal of the Iowa Academy of Science* 1992, *99*, 1-6.

(20) Hanson, C. D.; Castro, M. E.; Kerley, E. L.; Russell, D. H. *Analytical Chemistry* 1990, *62*, 520-526.

(21) Francl, T. J.; Sherman, M. G.; Hunter, R. L.; Locke, M. J.; Bowers, W. D.; McIver, R. T., Jr. *International Journal of Mass Spectrometry and Ion Processes* 1983, *54*, 189-199.

(22) Mitchell, D. W.; Smith, R. D. *Journal of Mass Spectrometry* 1996, *31*, 771-790.

(23) Peurrung, A. J.; Kouzes, R. T. *International Journal of Mass Spectrometry and Ion Processes* 1995, *145*, 139-153.

(24) Wong, R. L.; Amster, I. J. *International Journal of Mass Spectrometry* 2007, *265*, 99-105.

(25) Dunbar, R. C.; Chen, J. H.; Hays, J. D. *International Journal of Mass Spectrometry and Ion Processes* 1984, *57*, 39-56.

(26) Allemann, M.; Kellerhals, H. P.; Wanczek, K. P. *Chemical Physics Letters* 1981, *84*, 547-551.

(27) Nikolaev, E. N.; Rakov, V. S.; Futrell, J. H. *International Journal of Mass Spectrometry and Ion Processes* 1996, *157/158*, 215-232.

(28) Solouki, T.; Emmett, M. R.; Guan, S.; Marshall, A. G. *Analytical Chemistry* 1997, *69*, 1163-1168.

(29) Marshall, A. G.; Hendrickson, C. L.; Jackson, G. S. *Mass Spectrometry Reviews* 1998, *17*, 1-35.

(30) Jeffries, J. B.; Barlow, S. E.; Dunn, G. H. *International Journal of Mass Spectrometry and Ion Processes* 1983, *54*, 169-187.

(31) Vartanian, V. H.; Laude, D. A. *International Journal of Mass Spectrometry* 1998, *178*, 173-186.

(32) Shi, S. D. H.; Hendrickson, C. L.; Marshall, A. G. *Proceedings of the National Academy of Sciences of the United States of America* 1998, *95*, 11532-11537.

(33) Kaiser, N. K.; Bruce, J. E. *International Journal of Mass Spectrometry* 2007, *265*, 271-280.

Chapter II: Trapping Ring Electrode Cell

Abstract:

A novel FT-ICR cell called the trapping ring electrode cell (TREC) has been conceived, simulated, developed, and tested. The performance of TREC is compared to a closed cylindrical cell at different excited cyclotron radii. TREC permits the ability to maintain coherent ion motion at larger initial excited cyclotron radii by decreasing the change in radial electric field with respect to *z*-axis position in the cell. This is accomplished through post-excitation modulation of the trapping potentials applied to segmented trap plates. Resolving power approaching the theoretical limit was achieved using the novel TREC technology; over 420,000 resolving power was observed on melittin $[M+4H]^{4+}$ species when employed under modest magnetic field strength (3T). A tenfold gain in signal-to-noise ratio (S/N) is demonstrated over the closed cylindrical cell optimized with common potentials on all ring electrodes. The observed frequency drift during signal acquisition over long time periods was also significantly reduced, resulting in improved resolving power.

Introduction:

Fourier transform ion cyclotron resonance mass spectrometry[1] (FT-ICR-MS) provides high resolution, mass measurement accuracy, and sensitivity which makes it ideally suited for analytical application in the areas of proteomics[2-4], metabolomics[5], petroleomics[6, 7], and many others. FT-ICR-MS is the high performance end of proteomics research today, with the capability to identify proteins and protein-protein interactions based on peptide mass fingerprinting[8-10]. In general, the more accurately a mass can be determined, the more confident identification can be assigned for a given protein[11, 12] and the more confidently unknown peptide sequences can be determined[13]. The goal to apply mass spectrometry to ever-increasingly complex biological samples further increases the demand for increased analytical capabilities and the need for development of higher performance instrumentation.

The FT-ICR mass spectrometer relies upon an electromagnetic ion trap or cell to confine ions during detection[14-16]. The confinement is accomplished radially (*x*-*y* dimension) by an applied magnetic field parallel to the *z*-axis of the ion trap and axially using DC electrical potentials applied to trapping electrodes. As an ion approaches either trap plate, it experiences a force due to the electric field, and its kinetic energy is converted to potential energy. Thus, the ion exhibits periodic motion similar to the classical harmonic oscillator. As a consequence of the method by which ions are trapped within the cell, four natural motions arise. Trapping oscillation is the motion in which the ions oscillate in the z-dimension of the cell. Cyclotron motion is caused by the Lorentz force and is dependent upon the mass-to-charge ratio (*m*/*z*) (Equation 1).

$$\omega_c = \frac{qB_o}{m} = \frac{zeB_o}{m} \qquad (1)$$

Where ω_c is the cyclotron frequency, *z* is number of charges, *e* is the charge of an electron, B_o is the magnetic field strength, and *m* is the mass. Equation 1 represents the unperturbed cyclotron frequency, which is only dependent upon the *m*/*z* of the ion and the magnetic field strength. The third motion, magnetron motion, is caused by the outward directed radial component of the electrostatic field confining the ions in finite FT-ICR cells[17]. The radial electric field is perpendicular to the magnetic field and results in the $\vec{E} \times \vec{B}$ drift of the ions around the center of the ICR cell. Ion cloud rotation, the final of the four natural motions, results from the electric field generated by the ion cloud itself[18].

Signal duration, and consequently performance, in FTICR-MS is influenced by many factors, but the two most notable contributors to decreased signal duration are collisional damping[19] and ion-cloud dephasing[18]. Collisional damping is a signal decay process which is proportional to pressure; therefore, reducing the pressure in the cell region decreases signal decay, due to fewer collisions. The coherent motion of ions of a given *m*/*z* after initial excitation to some cyclotron orbit will induce an image current on the detection electrodes. As ions become increasingly out of phase, the image current decreases in

magnitude and is lost when equal numbers of ions of the same *m*/*z* are 180^{o} out of phase in their cyclotron orbit. This dephasing process is thought to be caused by a culmination of effects. The three which have been documented: magnetic field inhomogeneity, electric field inhomogeneity[20-22], and Coulombic interactions[23-26] occurring between ion clouds of differing *m*/*z*. Additionally, the applied electrical potentials in the trapping region of the cell result in a component of the electric field acting upon the ions radially. This radially outward directed force is one of the major mechanisms thought to be responsible for ion cloud dephasing (magnetron motion)[27-29]. Many high resolution FT-ICR measurements employ relatively low trapping potentials in order to minimize electric field inhomogeneity and its deleterious effect on coherent ion motion[30, 31]. The use of low trapping potentials requires that the ions entering the cell have sufficiently low kinetic energy to remain confined. Collisional cooling is a method of thermalizing ion kinetic energy; however, the undesirable pump-down time required to regain the low pressure needed for measurement ($\leq 10^{-9}$ torr) hinders high-throughput analysis. Magnetron frequency and space charge normally both reduce the observed cyclotron frequency as illustrated in Equation 2[32].

$$\omega_{obs.} = \omega_c - \omega_m - \delta \qquad (2)$$

In Equation 2, $\omega_{obs.}$, ω_c, ω_m, δ are the observed cyclotron frequency, the "unperturbed" cyclotron frequency, the magnetron frequency, and the collective effect of ion-ion interactions, respectively. It should be noted that the sign of the magnetron frequency term is dependent upon the direction of the radial component of the electric field force acting on an ion[33]. Outward-directed radial fields result in magnetron motion opposed to cyclotron motion, and thus, reduce the observed cyclotron frequency.

Maintaining coherent motion of the ion cloud within the ion trap is crucial to signal intensity and duration in an FT-ICR experiment[34], since the image current induced by the coherent ion packet diminishes as dephasing occurs. Thus, minimizing dephasing mechanisms can increase instrument

performance. A previous investigation by our laboratory demonstrated that reducing the outward directed force, which arises from the application of trapping potentials, has a favorable effect in that observed cyclotron frequency was shown to be independent of ion position along the *z*-axis within the cell[35]. Differences in reduced cyclotron frequency among ions (of the same *m*/*z*) with coherent cyclotron motion eventually leads to ion cloud dephasing and the decay of ICR signal with time.

A major limitation of current FT-ICR-MS instrumentation results from non-ideal electric fields present within the cell[31]. Electric fields are necessary, as previously mentioned, to confine the ions in the axial dimension, but the unfortunate artifact of finite cell geometry is a radially directed component of the electric field. The radial electric fields resulting from finite Penning traps have been of concern to investigators since the initial trapped cell experiments[15]. Two main solutions to improve the electric fields have been explored: segmentation of trapping electrode surfaces[36, 37] and changing the physical geometry of the cell[38-40]. Common ICR cell geometries include orthorhombic (cubic) and cylindrical (open and closed). Commercial instruments available today utilize the latter cell geometries (or a variation thereof). However, one must presently accept the unavoidable exchange in electric field homogeneity along the *z*-axis in the trapping region for non-linearity in the radio frequency excitation potential[38] with these cell designs. Other geometries exist, such as the hyperbolic cell[39, 40], which presents an example in which changing the geometry of the cell can result in an exactly quadrupolar trapping potential. The desirable attribute a quadrupolar field lends to an FT-ICR measurement is that cyclotron frequency is independent of radius. Most cell geometries approximate a quadrupolar field in a small region nearest to the center of the cell, but deviation from quadrupolar potential in cell geometries other than the hyperbolic cell becomes more severe as z-axis oscillation amplitude increases. However, even in a quadrupolar trapping well, the radial electric field variation over the oscillation amplitude results in different contributions of magnetron frequency to the observed cyclotron frequency.

Multiple approaches have been taken to linearize the radio frequency (RF) excitation potentials through variations of the orthorhombic and cylindrical cell[41, 42]. In the Infinity Cell, the trap plates are segmented in such a way as to approximate the excitation potential contours achieved with an infinitely long cylindrical cell. The capacitively coupled open cell has the RF excitation potential coupled to adjacent trapping electrodes. Both configurations were designed to produce linearization of the RF excitation potential. These designs reduce the problem of axial ejection of the ions due to *z*-axis excitation[43] and exemplify significant improvements over their predecessors, the closed cylindrical cell and the open cell. It should be recognized that both of the latter cell configurations have adopted the approach of linearizing the RF excitation profile and have not addressed the inhomogeneity in the radial electric field over the trapping region during the detection phase of ICR experiments.

Approaching the ICR cell problem from another perspective, one can seek to minimize electric field inhomogeneity. This approach serves to regulate the radial electric fields within the trapping region. It should be noted that this technique becomes most effective, as we shall see, when applied after the excitation of cyclotron motion. Wang and Marshall showed improvements in the ability to produce a nearly zero trap potential when a grounded screen is placed within a conventional orthorhombic cell[44]. They showed reduced variation in cyclotron frequency, reduced frequency shift, and higher mass measurement precision and accuracy with this cell modification. Although this design illustrates the importance of reducing radial electric fields, the weaker fields and grounded screen electrodes can decrease trapping efficiency in some cases.

The technique of "shimming" the electric fields in the cell using electrodes has been applied to the radial field problem recently by multiple investigators. Brustkern et al. developed a unique modification of the open coupled cell called the compensated cell[45]. This cell has three pairs of cylindrical compensation electrodes which are positioned in between the trapping and detection segments of the open coupled cell. With this cell impressive resolving power was demonstrated. A

similar modification of the open coupled cell by Tolmachev et al. using two sets of compensation electrodes between the trapping and excite/detect segments of the cell showed improved mass accuracy and allowed for excitation to larger cyclotron radius[46].

A cylindrical cell design with three pairs of circular electrodes spaced along the *z*-axis was developed by Naito *et al.*[47]. This cell was shown to have reduced radial electric field and to have a smaller drift (magnetron) frequency when compared to the conventional cylindrical cell. The authors conclude that the homogeneity of the electric field in the cell was increased by using annular electrodes to generate the trapping field. The potentials were independently manipulated and a variety of potential combinations were explored. The overarching notion accepted in practice, using the smallest trapping potential possible to achieve higher resolution, still seem to apply to this cell configuration.

Electron promoted ion coherence (EPIC), demonstrated previously by our laboratory, provided insight into the advantages behind regulating radial electric fields in the cell during detection[48]. The projection of an electron beam along the *z*-axis of an Infinity Cell[42] during detection resulted in a 3-5 fold increase in transient signal duration and resolution. Modeling in a subsequent study on the phenomenon revealed the electron beam to be favorably changing the electrostatic field in the trapping region[35]. The change in radial electric field over the trapping oscillation was significantly reduced.

A unique modification to the closed-cylindrical FT-ICR cell presented in this publication, TREC, is accomplished by segmentation of the trap plates into five concentric ring electrodes spatially positioned in the same plane as the original disc-like trap plate (Figure 1.1). These ring electrodes are independently controlled and modulated to a preset scheme following the excitation of the ions. This concept is contrasted to the design by Naito *et al.* in which the rings do not occupy the same plane and the potentials remain preset for an entire experiment (i.e., excitation, and detection). TREC provides the ability to tune the electrostatic fields to produce minimal change in the radial component over the ion axial oscillation at the initial excited cyclotron radius. Through the synergistic combination of theory and

(a) (b)

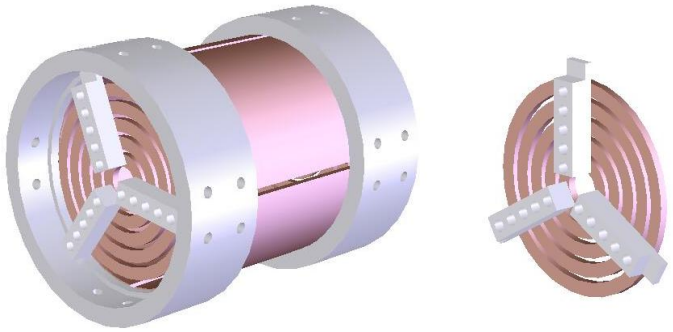

Figure 1.1 (a) A conceptual representation of the TREC. (b) The conceptual representation of a single TREC trap plate (magnified view).

experiment, we have shown that the TREC modification of the conventional closed cylindrical ion trap is beneficial for enhancing S/N ratio and resolving power of FT-ICR-MS. Other implications follow, such as increased cell capacity and the ability to excite ions to larger than conventional cyclotron radii. The observed enhancements are attributed to reduced radial electric field variation over the trapping oscillation of the ions.

Experimental:

TREC Design

The conceptual illustration and schematic for the first generation TREC design was rendered using SolidWorks 2004 (SolidWorks Corp., Suresnes, France). The ring electrodes were machined from solid oxygen free high conductivity (OFHC) copper. The braces, which ensure spatial uniformity and electrical isolation of the copper rings, were machined from MACOR machinable glass ceramic (Morgan Advanced Ceramics, Fairfield, NJ). The ring width is 0.110” and the spacing between each ring is 0.039”. The thickness of the rings is 0.063”. Machining tolerances for the MACOR braces and the copper ring electrodes are $\pm$ 0.005”. Commercially-pure titanium (CP-Ti) 2-56 socket cap screws (United Titanium, Wooster, OH) were used to fasten the MACOR braces to the ring electrodes and also serve as the terminals for wiring the DC potentials to the rings. All ten rings were wired separately, affording independent control over the DC potentials on each ring. Kapton coated wire (MDC Vacuum Products Corp., Hayward, CA) was used for electrical connections to the trapping ring electrodes. Tin-coated

copper ring-tongue solderless connectors (McMaster-Carr, Los Angeles, CA) were used to connect the Kapton wire to the terminals on the cell. The cell had an inner diameter of 1.875" and a length of 2" between trapping electrodes. All of the materials used in the construction of TREC were chosen with "outgassing" and magnetic field homogeneity as primary concerns.

TREC Operation

Generation of independently variable DC voltages for each of the ring electrodes was accomplished using a program developed in-house within LabVIEW 8.0. The process occurs through two computers working in concert, a MIDAS[49] data station and a computer housing the National Instruments hardware. Analog voltages are read in and digitized from the MIDAS data station through a NI board (NI PCI-6111, National Instruments, Austin, TX). These voltages are then supplied to all ten ring electrodes through another NI board (NI PCI-6723, National Instruments, Austin, TX) during all FT-ICR experimental events in which static or common potentials are applied. For the detection period, or any other period in which custom trap potential profiles are desired, the trapping rings are modulated to values (-10 V to +10 V) preset by the operator in the LabVIEW program. Switching from TREC to static (non-TREC) conditions is done using a transistor-transistor logic (TTL) trigger pulse from the MIDAS to the hardware computer. The variability in the switching times was observed using an oscilloscope and on average was ± 25 μs. This "jitter" in the time for voltage switching is negligible with respect to the detection interval and was acceptable for our experiments. From this point forth, non-TREC conditions (static conditions) will be defined as all rings having the same voltage applied during detection. TREC conditions will be defined as the modulated case in which the voltages are switched to a preset scheme during detection. Voltages will be listed in the order from smallest to largest ring electrode radius. For example, (0.2, 1.1, 1.6, 2.4, 2.8 V) will indicate the DC voltages applied to the five rings composing the front and rear trap plates from smallest to largest radius, respectively.

SIMION Modeling

Modeling of TREC was performed using SIMION 3D version 7.0 (D. A. Dahl, Idaho National Engineering and Environmental Laboratory). The model was designed to scale with the actual TREC design using 0.25 mm/grid unit and refined to a convergence level of 10^{-5}. Equipotential contour plots illustrate the approximate potentials within the cell during experiments with static or common voltages on all rings for both non-TREC and TREC conditions. Radial electric field plots were generated by recording the electric field component in the y-direction on an ion at millimeter increments across the cell at a given radius for both non-TREC and TREC conditions (~38% cell radius).

FT-ICR MS Experimental Conditions

The spectra presented here were obtained from a constructed-in-house 3.0 T Fourier transform ion cyclotron resonance mass spectrometer. This novel instrument will be discussed in a forthcoming publication[50], therefore, only the features relevant to the present data will be mentioned here. Electrospray ionization (ESI) was used as the source for all spectra presented. Ions were accumulated in a region of higher pressure in a quadrupole, then transferred to the cell via a set of RF-only quadrupoles. Spray solutions were composed of 49% ultrapure water (18 MΩ), 49% methanol (HPLC grade), and 2% acetic acid. Analyte concentrations for bradykinin, melittin, and ubiquitin (Sigma-Aldrich, St. Louis, MO) were 10 μM in spray buffer for all experiments. The ESI flow rate for all FT-ICR experiments was 1 μL/min. The potential on the ESI probe was defined as 2.5 kV and the flared capillary inlet[51] was placed at 200 V. The pressure in the cell region during all experiments was approximately 5 x 10^{-9} Torr.

In single scan experiments, ion cooling was accomplished by pulsing argon gas into the cell region for 1 ms followed by a 10 s pumping delay to remove excess neutrals prior to excitation. In experiments with static 1.1 V detection conditions, frequency swept excitation ranging from 20 kHz to 220 kHz with an amplitude of ~31 V_{p-p} was used to induce coherent cyclotron motion of the melittin ions. For the static 2.0 V detection conditions and TREC conditions (0.2, 1.1, 2.0, 2.4, and 2.8 V), frequency swept excitation ranging 20 kHz to 220 kHz with an amplitude of ~40 V_{p-p} was used to induce

coherent cyclotron motion of the melittin ions. The spectra shown were acquired at a sample rate of 160 kHz/s; 8 Megapoints of data were collected for each spectrum.

Radial dependence of signal intensity and S/N ratio of detected FT-ICR signals were investigated with single frequency excitation of bradykinin $[M+2H]^{2+}$ ions. Gated trapping was used to confine ion populations within the cell. A frequency of 87.4 kHz was applied for a total of 150 μs to induce coherent cyclotron motion of the ions. 64 K datapoints were collected at 160 kHz/s. For the S/N experiments, the excitation amplitude applied was ~20, 28, 33, and 39 V_{p-p}, corresponding to ~35, 45, 55, and 65% cell radius, respectively (calculated from single frequency version of equation 3). The voltage profiles selected for each excitation condition in the S/N plots were 35% (0.9, 1.0, 1.2, 1.6, and 2.0 V), 45% (0.8, 1.6, 2.0, 2.4, and 2.8 V), 55% (0.4, 1.2, 1.6, 2.0, and 2.4 V), and 65% (0.2, 0.8, 1.6, 2.0, and 2.4 V). Accumulation time was varied for each excitation condition from 0.1 to 1 second at each excitation condition. For the investigation of radial dependence on the signal intensity, the following various voltage profiles were applied to the trapping rings during detection: TREC 1 (0.8, 1.6, 2.0, 2.4, 2.8 V), TREC 2 (0.2, 0.8, 1.6, 2.0, 2.4 V), and TREC 3 (1.2, 1.4, 1.6, 2.0, 2.4 V). The names of these voltage profiles will be referred to without mention of the actual voltages henceforth for simplicity. Ion accumulation was set to 100 ms. Excitation amplitude was varied in 1.6 V_{p-p} increments.

All acquired FT-ICR data were analyzed with ICR-2LS[52]. The high resolution melittin data sets were subject to Fourier transform without any further processing; all the data except for the $[M+4H]^{4+}$ isotopic envelope was cleared. A subsequent reverse Fourier transform was applied to obtain the time domain signal isolated for the $[M+4H]^{4+}$ isotopic envelope.

Results and Discussion:

In previous studies with EPIC[35, 48], we showed an increase in FT-ICR-MS instrument performance. However, the observed cyclotron frequency was very sensitive to the number of electrons in the electron beam. The poor reproducibility of the number of electrons present during multiple

experiments proved inadequate for analytical applications with current hardware. Therefore, we have designed an FT-ICR cell that has the ability to tune radial electric fields, much like we observed with EPIC. In this new design, TREC, the flexibility and reproducibility in the resultant electrostatic fields are improved compared to what we observe with EPIC. The conceptual representation of TREC is shown in Figure 1a and 1b. A perspective view of the cell is shown in Figure 1a while Figure 1b is an enlargement of one segmented trap plate.

In viewing an equipotential contour plot, the electric field can be qualitatively obtained by the observer simply by envisioning the electric field to be orthogonal to the equipotential contour lines. If the slope of this electric field vector is zero with respect to *z*-axis there is no component of the electric field directed radially. When the slope is greater than zero some component of the electric field is directed radially (all of the electric field is directed radially when the slope is infinite). The radial electric field (-dV/dr) is defined as the component of the electric field orthogonal to the z-axis. Experimental comparison to the closed cylindrical cell can be made to a good approximation when static or common voltages are applied to the rings (non-TREC conditions). Figure 1.2a shows the equipotential contour plots produced by applying common 2.0 V potentials to all five rings in an effort to mimic the 2.0 V static conditions produced using a standard closed cylindrical cell design. The equipotential contour plot under TREC conditions with an applied potential scheme on the rings is shown in Figure 1.2b. Potentials applied on each ring with increasing electrode radius are 0.2, 1.1, 2.0, 2.4, and 2.8 volts, respectively. The key feature to compare between Figures 1.2a and 1.2b is the location in the cell where the change in radial electric field (-dV/dr) is minimized along the *z*-axis for either set of trapping conditions. In the case of the closed cylindrical cell, by imposing static conditions, the location where radial electric field is minimized occurs about 0% cell radius. This is good for minimizing magnetron motion at 0% cell radius, but this is not an advantageous electric field environment during detection, because ions orbit at some cyclotron radius (usually 30-50% cell radius). Decreasing the

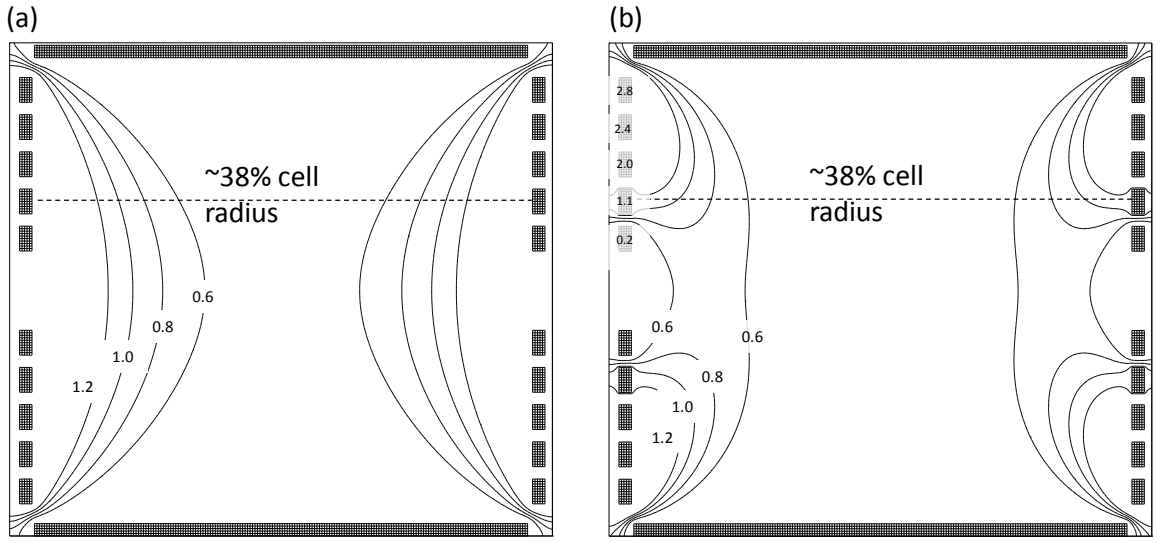

Figure 1.2: Equipotential contour plots are shown for (a) the static 2 V trapping conditions and (b) the TREC trapping conditions. The voltages for the modulated (TREC) trapping conditions with increasing electrode radius are 0.2, 1.1, 2.0, 2.4, and 2.8 volts respectively, as shown on the rings. A dashed line through the cell located at 38% cell radius is depicted.

radial electric field over ion *z*-axis oscillation is important to the overall performance of the cell because any component of the electric field not directed axially within the cell results in outward directed force acting upon the ions. Additionally, the radial electric field is proportional to the contribution of magnetron frequency to the observed cyclotron frequency. From the equipotential contour plots, we have demonstrated with TREC the ability to shift the position where the radial electric field has been minimized outward from the central axis of the cell, providing the region of decreased radial electric field at or near a given excited cyclotron radius. More importantly, this region can be tuned simply by changing the voltage modulation scheme appropriately.

The voltage modulation scheme applied to TREC in Figure 1.2b was first arrived at experimentally through multiple experimental iterations where the applied voltage to one pair of ring electrodes was independently varied until an optimal value was obtained for each ring. The nonlinear

DC voltage ramp was found through experiment to work well in a general sense, i.e., for all of the species analyzed with TREC. The equipotential contours generated from the voltage scheme arrived at experimentally share the same general feature of shifted region of minimized radial field when compared with results obtained previously by our laboratory through modeling EPIC[48]. Illustrated on both Figures 1.2a and 1.2b are the expected initial post-excitation cyclotron radius from Equation 1.3 for the melittin experiment expressed as a percentage of the inner diameter of the cell.

$$r_{excite} = \frac{\beta_{dipolar} V_{p-p} \sqrt{\frac{1}{Sweep\ Rate}}}{2dB_o} \qquad (3)$$

Where $\beta_{dipolar}$ is a geometry factor (the conventional closed cylindrical cell value was used[53];

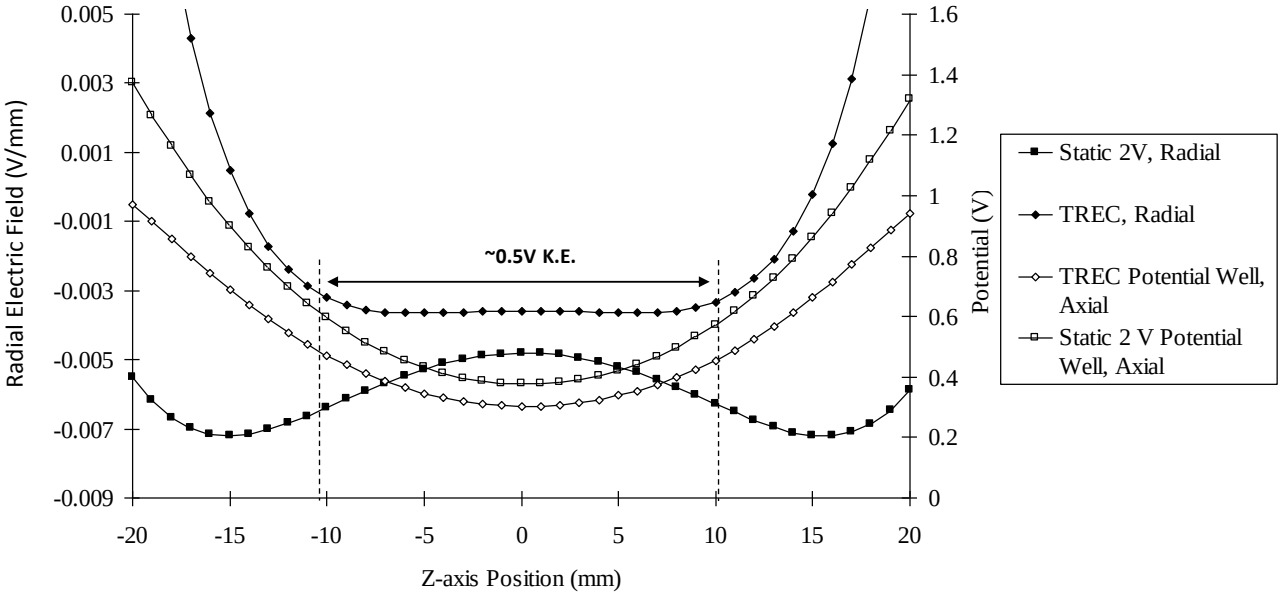

Figure 1.3: Radial electric field plots generated at 38% cell radius for both static 2 V trapping conditions and the TREC modulated conditions. A trapping potential well generated from the TREC conditions is overlaid to provide perspective.

$\beta_{dipolar}$ = 0.80818), $V_{p\text{-}p}$ is the applied excitation potential (V), the *sweep rate* refers to the rate that all excitation frequencies were applied (Hz/s), *d* is the distance between the trapping electrodes (m), and B_o is the magnetic field strength (T). This is only an approximation of the excited ion radius[31]; however, this approximation is adequate for the present discussion. A comparison of the radial electric field over the range of *z*-axis oscillation at 38% cell radius was generated in SIMION and depicted in Figure 1.3. The equipotential contours in Figure 1.2 correspond to the voltages applied to the trap plates during this experiment. The radial electric field variation over the *z*-axis is much greater with the static 2 V non-TREC conditions. The variation of the radial electric field under TREC conditions is nearly zero over an oscillation amplitude of -10 to 10 mm along the *z*-axis. The trapping well confining the ions in the *z* dimension is superimposed over the radial electric field plot. A reference point of 0.5 V kinetic energy is inscribed within the potential well to illustrate the oscillation amplitude of ions with a liberal amount of kinetic energy following collisional cooling. Certainly the *z*-axis kinetic energy of ion populations in the cell will vary; thus, the depth of penetration into the trapping fields will vary. However, the change in radial electric field over the same *z*-axis oscillation amplitude in a conventional closed cylindrical cell vs. TREC is demonstrated. This is true when considering any region in the central 2/3 of the cell. The voltage modulation scheme placed on the electrodes for this experiment may not be fully optimized. Nonetheless, utilizing TREC, we have illustrated the ability to minimize the change in radial fields over the *z*-axis oscillation of the ions at their excited cyclotron radius.

The comparison of a single scan spectrum collected with non-TREC and TREC conditions is provided in Figure 1.4 for melittin $[M+4H]^{4+}$ species. The extracted time-domain signals are provided, zeroing all points outside the *m*/*z* range of interest, to show the dramatic contrast in the data obtained with each set of trap plate conditions[54]. In general, additional techniques are used to process FT-ICR spectra, such as apodization or zero-filling. These processes augment peak shape and other characteristics of the spectrum; therefore, these techniques were not utilized in the data processing.

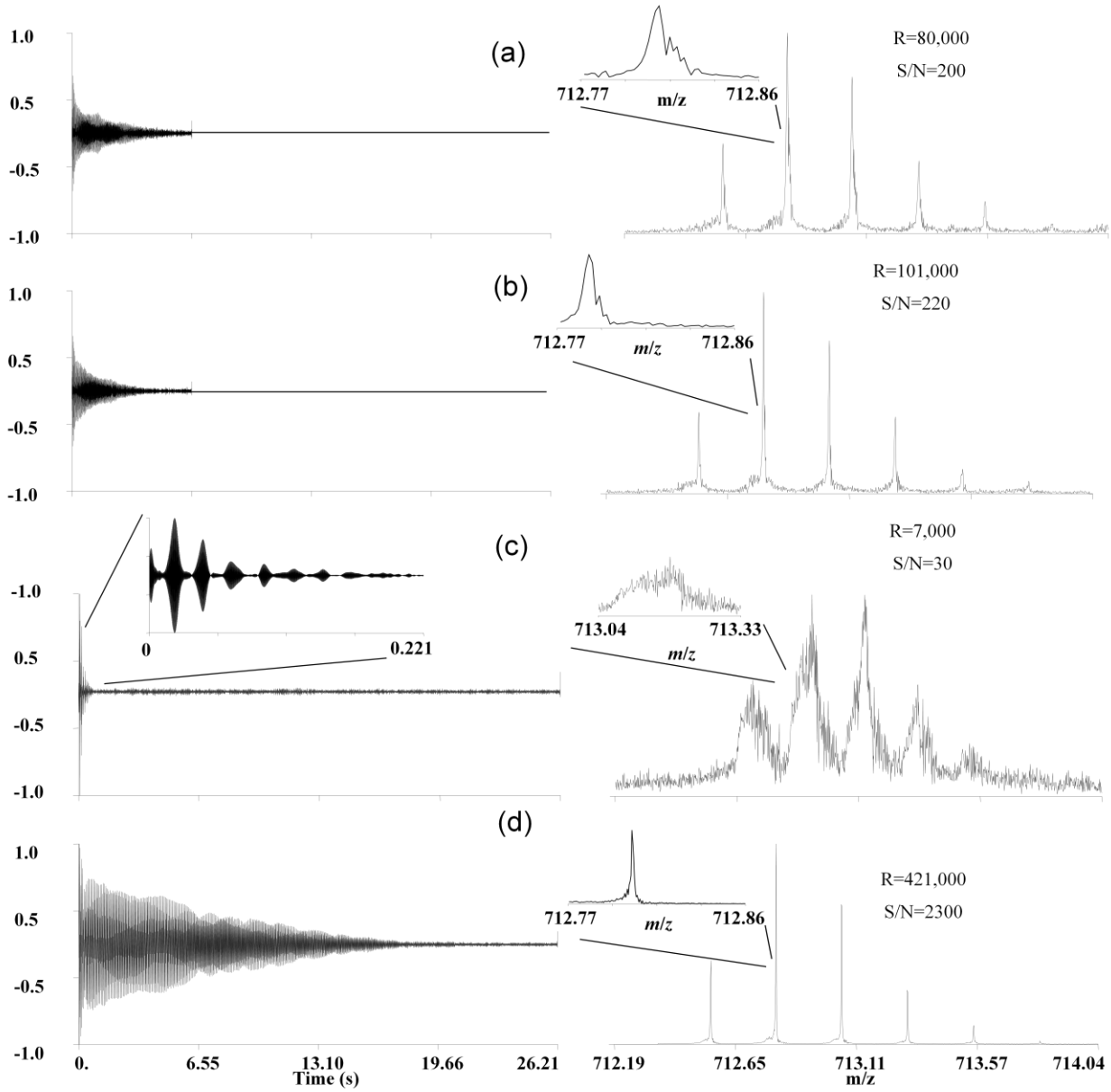

Figure 1.4: Comparison of melittin $[M+4H]^{4+}$ spectra acquired with static and the TREC conditions. (a) The spectrum collected with static 1.1 V conditions with increased ion population. (b) The spectrum collected with optimized 1.1 V conditions with a decreased ion population. (c) The spectrum collected with 2.0 V static conditions. (d) The spectrum collected using the TREC, modulating the voltages only during the detection phase. Inset shows the peak shape of the most abundant isotopic peak in each case.

Figure 1.4a and 1.4b are spectra in which static 1.1 V conditions were employed. These spectra were acquired varying instrumental parameters including trap plate voltages, accumulation time, and excitation amplitude. The spectra are shown to illustrate that the instrument can achieve respectable

performance (mass dependent resolving power in the range of 18,000-278,000[55-57]), as expected from a 3 T field strength. The difference between these two datasets is the ion population present during data acquisition. Figure 1.4a 1 ms ion accumulation time was used while Figure 1.4b 0.5 ms ion accumulation time was used. Figure 1.4c shows the transient signal and corresponding mass spectrum acquired with 2.0 V static conditions applied during detection. Figure 4d shows the transient signal and corresponding mass spectrum under TREC conditions in which the rings were modulated to the following voltages immediately following excitation: 0.2, 1.1, 2.0, 2.4, 2.8 V (voltage profile used in Figures 1.2 and 1.3). The spectra shown in Figure 1.4c and 1.4d were acquired under identical experimental conditions, except the voltage profile mentioned above was applied during the detection phase for the TREC spectrum. The dramatic increase in the transient signal length shown in Figure 1.4d is attributed to the decreased dephasing resulting from minimization of radial electric field differences and magnetron frequencies of the ions. Thus, ions of the same *m*/*z* ratio (but different z-axis KE) possess the same or nearly the same magnetron frequency contribution to the observed cyclotron frequency. Decreased variation in magnetron frequency in an ion population of a given *m*/*z* promotes coherent motion for a longer duration. Furthermore, when contrasting the static conditions with TREC conditions, we have demonstrated with TREC the ability to acquire long time-domain signals with relatively high trapping potentials. In addition, application of relatively high TREC potentials does not preclude high resolving power, as is normally observed with static, non-TREC experiments.

For example, the resolving power (FWHM) achieved using TREC in Figure 1.4d was 421,000. The resolving power of the non-TREC experiment with the same experimental parameters (Fig. 4c) showed 7,000. The comparison of TREC versus static 1.0 V conditions is revealed through Figures 1.4d and 1.4b respectively. In the optimized static experiment, average resolving power over the isotopic envelope was 101,000 (Fig. 1.4b). The resolution was averaged over all of the observable isotopic peaks contained in the isotope envelope for the $[M+4H]^{4+}$ species. The theoretical resolving power or the

highest achievable resolving power for the experiment can be approximated from the expression shown in equation 5[19].

$$R \cong \frac{f \cdot t}{2} \qquad (5)$$

Where *R* is the theoretical resolving power, *f* is the observed cyclotron frequency, and *t* is the time duration of the transient signal. The expected theoretical resolving power for this experiment is ~585,000. This indicates that with the TREC modification theoretical resolving power is approached (72% theoretical resolving power). The expected theoretical resolving power for the spectrum in 1.4b is 210,000, where 48% of theoretical resolving power was achieved. In data sets where the time domain signal has been truncated theoretical resolution is achieved. A transient signal collected over 13 s using the same TREC conditions (see Supplemental Figure 1) shown ~400,000 resolving power with the theoretical resolving power of 423,000 (95% theoretical resolving power). The concept of minimizing radial electric field variation about the excited cyclotron radius of the ions is highly dependent upon how accurately the cyclotron radius has been defined. Definition of the cyclotron radius is achieved through the excitation event in each ICR experiment. Therefore, gains in S/N and resolution using TREC are limited by the excitation event.

A four-fold increase in resolving power is achieved when comparing TREC and optimized non-TREC conditions (static 1.1 V). An important observation of the TREC spectrum is that the frequency does not drift with time over this long transient signal as noted in conventional ICR cells[58, 59]. An inset showing a magnified view of the most abundant isotope peak (Fig. 1.4) of the melittin $[M+4H]^{4+}$ species reveals little asymmetry in the peak shape for the TREC spectrum as compared with the non-TREC spectra. The "tailing" observed in the peaks shown for non-TREC conditions, (Figures 1.4a and 1.4b) indicates a shift in frequency over the data acquisition period. Frequency stability over the data acquisition time period is also thought to be responsible for the observed increase in performance using

TREC. A comparison of the S/N ratio in the spectra presented in Figure 1.4 shows a ten -fold improvement in TREC over optimized non-TREC spectra.

Improved S/N resultant from excitation to large cyclotron radii is possible because the signal intensity in FT-ICR is proportional to the proximity of ions to the detection electrodes. Sensitivity is fundamentally related to S/N. Investigation of the S/N in both the static and TREC conditions provides a uniquely genuine comparison, since the only experimental variable altered was the trapping voltage during detection. Quantification of the gain in S/N using TREC over non-TREC conditions is presented in Figure 1.5. SIMION was used to predict four voltage profiles for performance enhancement at the specified post-excitation cyclotron radius. The criterion used to select these voltage schemes was the electric field environment at or near the axial region of the excited cyclotron radius predicted by Equation 3. A direct comparison, the change in S/N with TREC over non-TREC conditions, is depicted in Figure 1.5. Overall, approximately a ten-fold gain in S/N is achieved with TREC over static 2.0 V conditions in the range of radii studied (35%-65% cell radius).

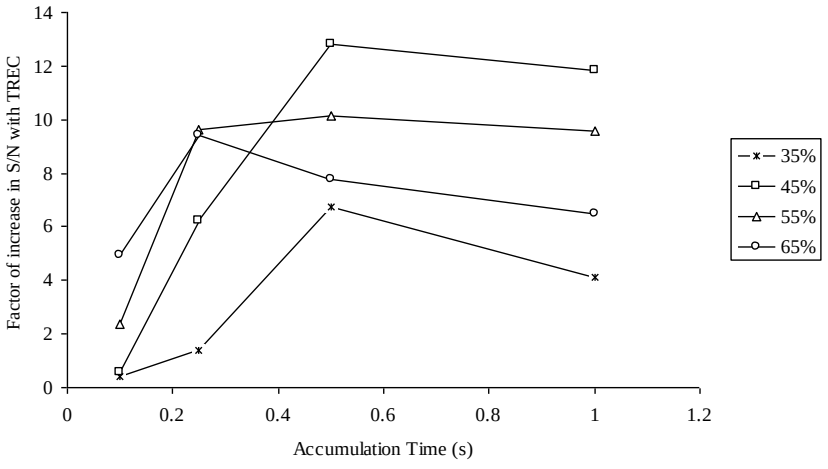

Figure 1.5: The change in S/N of the TREC over static 2.0 V conditions is shown. A tenfold increase in S/N is achieved using the TREC technology over the radii studied (35%-65% cell radius).

The ability to tune the electrical potentials for decreased radial electric field variation over the axial oscillation is an important feature of TREC which enables the performance improvements demonstrated. This tunability is experimentally represented in Figure

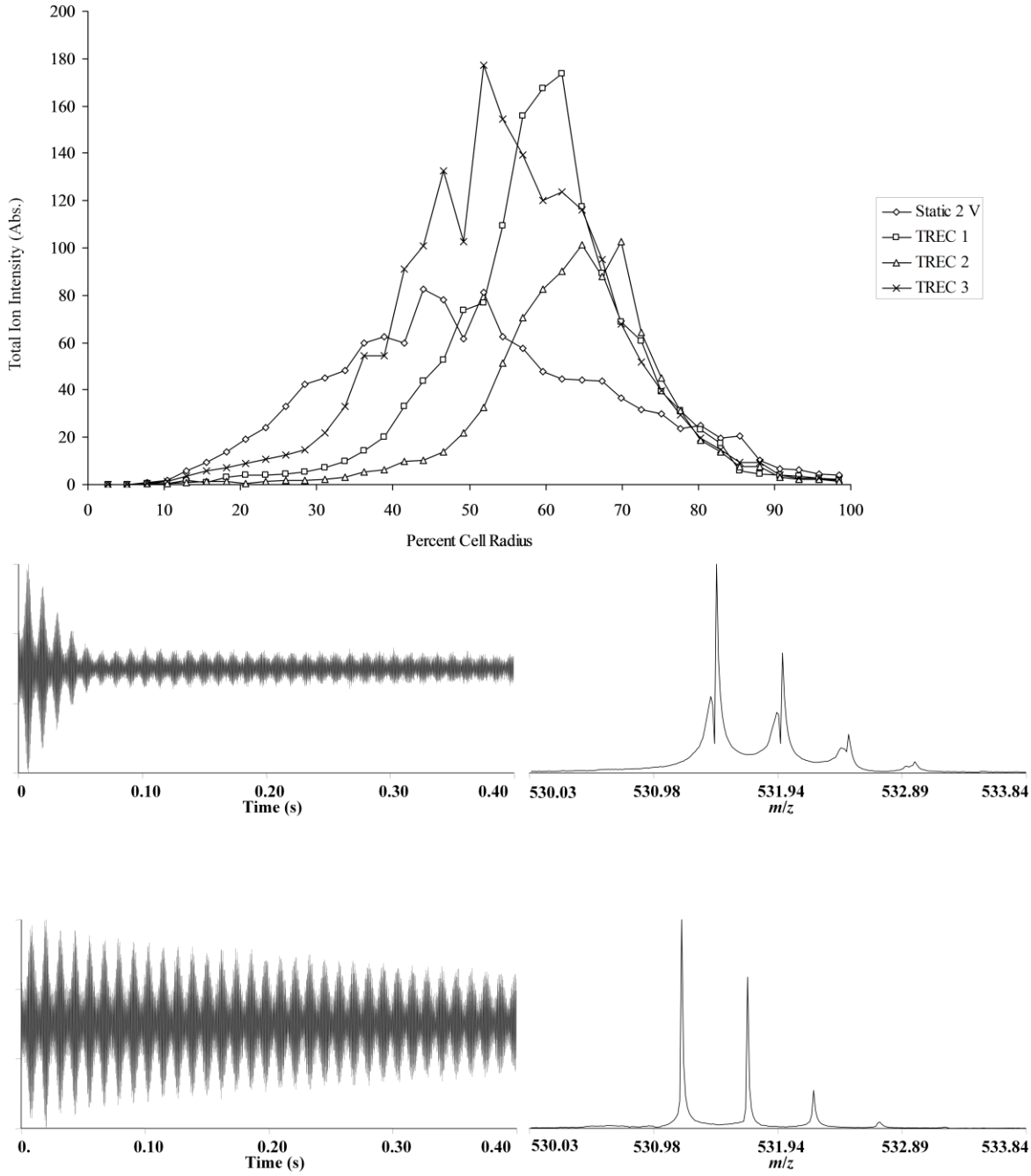

Figure 1.6: The plot in (a) shows the total ion intensity (absolute) of the bradykinin $[M+2H]^{2+}$ isotopic envelope vs. % cell radius for static 2 V trapping compared to a variety of TREC voltage profiles. In (b), a representative spectrum is shown using single frequency excitation of bradykinin $[M+2H]^{2+}$ for static 2 V conditions. In (c), a representative spectrum is shown using single frequency excitation of bradykinin $[M+2H]^{2+}$ for the TREC 3 conditions (1.2, 1.4, 1.6, 2.0, 2.4 V).

1.6. These data were generated using single frequency excitation of bradykinin $[M+2H]^{2+}$ with the excitation amplitude being varied incrementally. Each data point is a signal average of ten consecutive

scans. Data acquisition was truncated to 0.4 s for each scan, as high resolution was not of primary importance to the results. The total ion intensity (absolute) was summed over the isotopic envelope, with a threshold of three times the S/N. Initial post-excitation cyclotron radii were generated using the single frequency version of Equation 3. Using single frequency excitation, the approximation this equation provides appears to hold; at the boundary of the cell (100% cell radius) the signal plummets to zero intensity. The three TREC profiles, TREC 1, TREC 2, and TREC 3, have a different post-excitation radius for which enhancement in ion intensity appears the strongest, ~62%, 70%, and ~52% cell radius, respectively. An interesting observation in these data is that at low cyclotron radii, ~39% cell radius and smaller, the static 2 V condition shows higher ion intensity. This can be predicted by considering the equipotential contours produced with common 2 V potentials placed on all of the rings. The region in the cell where the radial electric field variation is the smallest is centered about 0% cell radius. Using the TREC voltage profiles designed for this experiment actually would create a radially inward directed electric field component in which the magnitude would increase as 0% cell radius was approached.

This experiment also reveals the ability of TREC to provide enhancement on the throughput timescale necessary for LC-MS analysis. Figures 1.6b and 1.6c are shown for comparison at maximum ion intensity for both static 2 V and the TREC 3 conditions. The damping rate in the transient signals for both experiments is dramatically different. This is apparent in the spectral quality, considering resolution and S/N of the spectra in Figure 1.6. The high duty-cycle demand that LC-MS places on an instrument make it difficult to achieve high performance and high throughput simultaneously, so the instrument performance enhancements TREC provides make it valuable to this type of analysis.

It must be mentioned that although the current TREC design (Figure 1.1), which consists of five ring electrodes, can minimize radial fields near the expected post-excitation cyclotron radius, a design containing more than five independently controlled electrodes would impart better definition and control over the potentials within the trapping region. The current TREC design is focused on producing

electric fields ideally suited for detection, and we have not addressed in the design its susceptibility to z-axis ejection during excitation. However, the TREC design is compatible with the Infinity Cell[42] concept or a similar approach where excitation has been coupled to the segmented trap plates. Integrating the TREC concept with excitation coupled to the trapping ring electrodes would address *z*-axis ejection[41] and linearize the excitation profile, while retaining the ability to moderate the radial electric fields during detection.

Conclusion

Through the theory, development, and implementation of TREC, performance of FTICR-MS was greatly increased. TREC is one novel component in an original FTICR-ICR mass spectrometer being developed by our laboratory. The resolution was increased by greater than a factor of four over optimized non-TREC conditions (static 1.1 V) and potentially can be further optimized for additional gain. The S/N was shown to be increased by a factor of ten over static trapping conditions. The mechanism for the gain in performance has been shown to occur by mitigating the change in radial electric field in the region of the post-excitation cyclotron motion of the ions. In addition, it was shown that tuning the radius for which the greatest enhancement in signal is applied (~50-70% cell radius) is possible with TREC, simply by altering the voltage profile applied after excitation of ion cyclotron motion. This technology is flexible and can be implemented on commercial instruments. It is expected that the enhancements provided with the new TREC technology will be scalable to the magnetic field utilized. Convolving TREC with the concept of coupled RF excitation to the trap plate segments will provide an ICR cell which effectively addresses linearization of excitation potential and reduction in the change in radial electric field over ion oscillation. TREC also may provide a unique opportunity to study the effects of space charge and image charge with a decreased perturbation due to coherent ion motion via decreased difference in magnetron frequency.

Acknowledgements

The authors acknowledge Alan Marshall and his group at the National High Magnetic Field Laboratory for the use of the MIDAS data station. This material is based upon work supported by the Directorate of Biological Sciences, National Science Foundation under Grant No. 0352451; Murdock Charitable Trust; and Office of Science (BER), U.S. Department of Energy, Grant No. DE-FG02-04ER63924.

Works Cited

(1) Comisarow, M. B.; Marshall, A. G. *Chemical Physics Letters* 1974, *25*, 282-283.

(2) Henry, K. D.; Williams, E. R.; Wang, B. H.; McLafferty, F. W.; Shabanowitz, J.; Hunt, D. F. *Proc Natl Acad Sci U S A FIELD Full Journal Title:Proceedings of the National Academy of Sciences of the United States of America* 1989, *86*, 9075-9078.

(3) Kelleher, N. L.; Nicewonger, R. B.; Begley, T. P.; McLafferty, F. W. *J Biol Chem FIELD Full Journal Title:The Journal of biological chemistry* 1997, *272*, 32215-32220.

(4) Olsen Jesper, V.; Mann, M. *Proc Natl Acad Sci U S A FIELD Full Journal Title:Proceedings of the National Academy of Sciences of the United States of America* 2004, *101*, 13417-13422.

(5) Brown, S. C.; Kruppa, G.; Dasseux, J.-L. *Mass Spectrometry Reviews* 2005, *24*, 223-231.

(6) Rodgers, R. P.; Schaub, T. M.; Marshall, A. G. *Analytical Chemistry* 2005, *77*, 20A-27A.

(7) Marshall, A. G.; Rodgers, R. P. *Accounts of Chemical Research* 2004, *37*, 53-59.

(8) Bossio Robert, E.; Marshall Alan, G. *Anal Chem FIELD Full Journal Title:Analytical chemistry* 2002, *74*, 1674-1679.

(9) Tang, X.; Munske, G. R.; Siems, W. F.; Bruce, J. E. *Analytical Chemistry* 2005, *77*, 311-318.

(10) Lipton, M. S.; Pasa-Tolic, L.; Anderson, G. A.; Anderson, D. J.; Auberry, D. L.; Battista, J. R.; Daly, M. J.; Fredrickson, J.; Hixson, K. K.; Kostandarithes, H.; Masselon, C.; Markillie, L. M.; Moore, R. J.; Romine, M. F.; Shen, Y.; Stritmatter, E.; Tolic, N.; Udseth, H. R.; Venkateswaran, A.; Wong, K.-

K.; Zhao, R.; Smith, R. D. *Proceedings of the National Academy of Sciences of the United States of America* 2002, *99*, 11049-11054.

(11) He, F.; Emmett, M. R.; Hkansson, K.; Hendrickson, C. L.; Marshall, A. G. *Journal of Proteome Research* 2004, *3*, 61-67.

(12) Goodlett, D. R.; Bruce, J. E.; Anderson, G. A.; Rist, B.; Pasa-Tolic, L.; Fiehn, O.; Smith, R. D.; Aebersold, R. *Analytical Chemistry* 2000, *72*, 1112-1118.

(13) Spengler, B. *Journal of the American Society for Mass Spectrometry* 2004, *15*, 703-714.

(14) Dehmelt, H. *Reviews of Modern Physics* 1990, *62*, 525-530.

(15) McIver, R. T., Jr. *Review of Scientific Instruments* 1970, *41*, 555-558.

(16) Penning, F. M. *Nederlands Tijdschrift voor Natuurkunde (1934-1976)* 1936, *3*, 141-154.

(17) Marshall, A. G.; Guan, S. *Physica Scripta, T* 1995, *T59*, 155-164.

(18) Peurrung, A. J.; Kouzes, R. T. *Physical Review E: Statistical Physics, Plasmas, Fluids, and Related Interdisciplinary Topics* 1994, *49*, 4362-4368.

(19) Marshall, A. G.; Comisarow, M. B.; Parisod, G. *Journal of Chemical Physics* 1979, *71*, 4434-4444.

(20) Mitchell, D. W.; Hearn, B. A.; DeLong, S. E. *International Journal of Mass Spectrometry and Ion Processes* 1993, *125*, 95-126.

(21) Capron, M. A.; Haskin, S. S.; Hanson, C. D. *Journal of the Iowa Academy of Science* 1992, *99*, 1-6.

(22) Hanson, C. D.; Castro, M. E.; Kerley, E. L.; Russell, D. H. *Analytical Chemistry* 1990, *62*, 520-526.

(23) Francl, T. J.; Sherman, M. G.; Hunter, R. L.; Locke, M. J.; Bowers, W. D.; McIver, R. T., Jr. *International Journal of Mass Spectrometry and Ion Processes* 1983, *54*, 189-199.

(24) Mitchell, D. W.; Smith, R. D. *Journal of Mass Spectrometry* 1996, *31*, 771-790.

(25) Peurrung, A. J.; Kouzes, R. T. *International Journal of Mass Spectrometry and Ion Processes* 1995, *145*, 139-153.

(26) Wong, R. L.; Amster, I. J. *International Journal of Mass Spectrometry* 2007, *265*, 99-105.

(27) Dunbar, R. C.; Chen, J. H.; Hays, J. D. *International Journal of Mass Spectrometry and Ion Processes* 1984, *57*, 39-56.

(28) Allemann, M.; Kellerhals, H. P.; Wanczek, K. P. *Chemical Physics Letters* 1981, *84*, 547-551.

(29) Nikolaev, E. N.; Rakov, V. S.; Futrell, J. H. *International Journal of Mass Spectrometry and Ion Processes* 1996, *157/158*, 215-232.

(30) Solouki, T.; Emmett, M. R.; Guan, S.; Marshall, A. G. *Analytical Chemistry* 1997, *69*, 1163-1168.

(31) Marshall, A. G.; Hendrickson, C. L.; Jackson, G. S. *Mass Spectrometry Reviews* 1998, *17*, 1-35.

(32) Jeffries, J. B.; Barlow, S. E.; Dunn, G. H. *International Journal of Mass Spectrometry and Ion Processes* 1983, *54*, 169-187.

(33) Vartanian, V. H.; Laude, D. A. *International Journal of Mass Spectrometry* 1998, *178*, 173-186.

(34) Shi, S. D. H.; Hendrickson, C. L.; Marshall, A. G. *Proceedings of the National Academy of Sciences of the United States of America* 1998, *95*, 11532-11537.

(35) Kaiser, N. K.; Bruce, J. E. *International Journal of Mass Spectrometry* 2007, *265*, 271-280.

(36) Vartanian, V. H.; Hadjarab, F.; Laude, D. A. *International Journal of Mass Spectrometry and Ion Processes* 1995, *151*, 175-187.

(37) Kanawati, B.; Wanczek, K. P. *Review of Scientific Instruments* 2007, *78*, 074102/074101-074102/074108.

(38) Guan, S.; Marshall, A. G. *International Journal of Mass Spectrometry and Ion Processes* 1995, *146/147*, 261-296.

(39) Rempel, D. L.; Ledford, E. B., Jr.; Huang, S. K.; Gross, M. L. *Anal Chem FIELD Full Journal Title:Analytical chemistry* 1987, *59*, 2527-2532.

(40) Yin, W. W.; Wang, M.; Marshall, A. G.; Ledford, E. B., Jr. *Journal of the American Society for Mass Spectrometry* 1992, *3*, 188-197.

(41) Beu, S. C.; Laude, D. A., Jr. *Analytical Chemistry* 1992, *64*, 177-180.

(42) Caravatti, P.; Allemann, M. *Organic Mass Spectrometry* 1991, *26*, 514-518.

(43) Van der Hart, W. J.; Van de Guchte, W. J. *International Journal of Mass Spectrometry and Ion Processes* 1988, *82*, 17-31.

(44) Wang, M.; Marshall, A. G. *Analytical Chemistry* 1989, *61*, 1288-1293.

(45) Brustkern, A. M.; Rempel Don, L.; Gross Michael, L., Indianapolis, IN 2007.

(46) Tolmachev, A. V.; Robinson, E. W.; Wu, S.; Kang, H.; Lourette, N. M.; Pasa-Tolic, L.; Smith, R. D. *Journal of the American Society for Mass Spectrometry* 2008, *In Press*.

(47) Naito, Y.; Fujiwara, M.; Inoue, M. *International Journal of Mass Spectrometry and Ion Processes* 1992, *120*, 179-192.

(48) Kaiser, N. K.; Bruce, J. E. *Analytical Chemistry* 2005, *77*, 5973-5981.

(49) Senko, M. W.; Canterbury, J. D.; Guan, S.; Marshall, A. G. *Rapid Communications in Mass Spectrometry* 1996, *10*, 1839-1844.

(50) Kaiser, N. K., et al 2008.

(51) Wu, S.; Zhang, K.; Kaiser, N. K.; Bruce, J. E.; Prior, D. C.; Anderson, G. A. *Journal of the American Society for Mass Spectrometry* 2006, *17*, 772-779.

(52) Anderson, G. A.; Bruce, J. E.; Smith, R. D.*,* 2.18 ed.: Richland, WA, 1996.

(53) Jackson, G. S.; Canterbury, J. D.; Guan, S.; Marshall, A. G. *Journal of the American Society for Mass Spectrometry* 1997, *8*, 283-293.

(54) Bresson, J. A.; Anderson, G. A.; Bruce, J. E.; Smith, R. D. *Journal of the American Society for Mass Spectrometry* 1998, *9*, 799-804.

(55) McCullough, S. M.; Gard, E.; Lebrilla, C. B. *International Journal of Mass Spectrometry and Ion Processes* 1991, *107*, 91-102.

(56) Polfer, N. C.; Haselmann, K. F.; Zubarev, R. A.; Langridge-Smith, P. R. R. *Rapid Communications in Mass Spectrometry* 2002, *16*, 936-943.

(57) Gooden Jonathon, K.; Rempel Don, L.; Gross Michael, L. *J Am Soc Mass Spectrom FIELD Full Journal Title:Journal of the American Society for Mass Spectrometry* 2004, *15*, 1109-1115.

(58) Bruce, J. E.; Anderson, G. A.; Hofstadler, S. A.; Winger, B. E.; Smith, R. D. *Rapid Communications in Mass Spectrometry* 1993, *7*, 700-703.

(59) Guan, S.; Wahl, M. C.; Marshall, A. G. *Analytical Chemistry* 1993, *65*, 3647-3653.

Chapter III: eTREC: excite-coupled Trapping Ring Electrode Cell

Abstract:

A novel excite-coupled Trapping Ring Electrode Cell (eTREC) was designed and developed. eTREC technology provides greater linearity in the excitation electric field along with minimized variation in radial trapping field during detection. The variation in the radial trapping electric field is reduced through post excitation modulation of the trapping potentials applied to the Trapping Ring Electrode Cell (TREC). Linearization of the electric field generated during radio frequency (RF) excitation is accomplished by coupling the RF excitation to a novel electrode arrangement superimposed onto the trapping rings of a TREC. The coupling of RF excitation to the trap plates effectively reduces z-axis ejection and allows for a more uniform post-excitation radius for the entire ion population. Using this technology sensitivity was increased by >50%, resolution of $^{13}C_2$ and ^{34}S fine structure peaks was achieved with the peptide MMMMG (~330,000 RP) on a 3 Tesla system, and the limit of detection was significantly reduced.

Introduction:

Fourier Transform Ion Cyclotron Resonance Mass Spectrometry (FTICR-MS)[1] is a high performance technique capable of simultaneous high resolution, high mass measurement accuracy, wide dynamic range, and high sensitivity measurements[2-5]. FT-ICR-MS continues to be used in many fields to solve difficult problems. Analysis of complex samples acquired from the fields of proteomics[6, 7], metabolomics[8, 9], petroleomics[10, 11], and others require instrumentation of the highest performance to extract the maximum amount of information possible. Few instruments meet the performance demands imposed by the aforementioned fields of interest; however, FTICR-MS has been routinely applied in these areas due to its extraordinary performance criteria.

In spite of its outstanding attributes, FTICR-MS technology requires further development to realize its fullest potential. Performance limitations such as radial electric field variation in the cell and

mass discrimination during ion transmission are still areas of FTICR-MS technology which require improvement. The most recent efforts from our laboratory to improve FTICR-MS performance have been focused on ion transmission[12] and ion detection[13]. The data presented in this manuscript has a focus on ion detection. The heart of FTICR-MS is the cell which is used for confinement and *m/z* analysis. Fine details of cell operation and the many incarnations of the ICR cell[3, 13-21] are the focus of review articles[22, 23]. Ion confinement in all cells is achieved through the application of an axial electric field and a uniform magnetic field. Ions that reach the cell and are trapped have a distribution or spread in trapped ion kinetic energy. A spread in trapped ion kinetic energy leads to a spread in the extent of z-axis oscillation within the cell. The spread in trapped ion kinetic energy is present before and after ion excitation and during the detection process. Radial electric field varies along the z-axis at the post-excitation cyclotron radius (r_c) even in cells developed to have quadrupolar or harmonic trapping potentials (ideal electric field environment). Therefore, ions of the same *m/z*, but different z-axis kinetic energy, experience a distribution in radial electric field during ion detection. Radial electric field magnitude defines magnetron frequency. Ions of the same *m/z*, but different z-axis kinetic energy, will have a distribution in magnetron frequencies which arises from the variation in radial field[24]. The detected or observed ion cyclotron frequency (ω_o) is related to the "unperturbed" cyclotron frequency (ω_+) and magnetron frequency(ω_-) through the following expression[23]:

$$\omega_o = \omega_+ - \omega_- \qquad (1)$$

Contribution of magnetron frequency to the observed frequency is orders of magnitude smaller than the cyclotron frequency for the *m/z* regime most commonly analyzed; however, relatively small frequency differences result in rapid ion cloud dephasing or distorted peak shape. The excitation event defines the initial phase coherence of cyclotron motion. Therefore, ions of the same *m/z* begin in phase, but due to slight differences in magnetron frequency ions lose phase coherence, and consequently, signal loss is

observed[25]. There are other mechanisms for signal loss in ICR experiments such as collisional damping; however, these contributions are normally minimized by operation at low background pressure.

Our studies of electron promoted ion coherence (EPIC)[24-26] showed that radial electric fields are very important for control of ion cloud dephasing, and thus, can strongly affect instrument performance. The effect of radial electric field variation on cell performance was also observed by Kim et al. upon inversion of the sidekick potential of an Infinity cell during detection[27]. Further investigation into the radial field effects on trapped ion kinetic energy in an Infinity cell have indicated that the extent of oscillation has a profound impact on observed frequency. Specifically, ion populations of the same *m/z* with different pre-excitation z-axis kinetic energy[24] are observed at different cyclotron frequencies. The difference in observed frequency between "hot" and "cool" ion populations of the same m/z was eliminated through the application of EPIC, which modulates the radial fields during ion detection. Development of a cell with the capability to minimize radial electric field variation at the cyclotron radius (r_c) has provided further support of the hypothesis that radial field variation along the z-axis at the post excitation cyclotron radius dramatically influences instrument performance[13]. Using TREC, we observed a 10-fold gain in signal intensity, decreased ion frequency drift, and resolving power near the theoretical limit. Although our experimentation with the initial Trapping Ring Electrode Cell (TREC) supported the radial field variation hypothesis, no method for correcting non-ideal excitation fields was incorporated in this design.

The coupling of RF excitation to the trapping electrode surfaces of the ICR cell has been demonstrated by multiple researchers and has been integrated into commercial instruments[14, 17, 28, 29]. The motive for incorporating excitation coupling is to correct for non-ideality in the electric field present during the excitation event. The finite geometry of the closed cell design causes deviation in excite potentials at the extremes of the cell (near the end-cap electrodes, or near the edge of the excite/detect electrodes). This deviation results in a component of the electric field directed axially, and thus,

provides an undesirable excitation of the z-axis oscillation of the ion cloud[30]. Excitation of the z-axis motion can cause ejection from the cell and/or provide a poorly defined cyclotron radius (increase in z-x spread). This phenomenon has long been recognized and surmounted in a variety of ways[14, 17, 29, 31].

An ideal dipolar excitation field is produced in the limit of infinite cell length. In the plane which bisects the excitation electrodes axially, the shape of this field is linear as a function of increasing radius without regard to z displacement. An important consequence of finite excitation electrodes in all cell designs is that they effectively short the RF potential applied to ground at their boundaries. The result is that the excitation field changes greatly as a function of z displacement in uncoupled cell designs. In the limit of infinite cell radius the trapping radial electric field variation along the z-axis at any cyclotron radius would be zero. An important consequence of finite trapping electrodes is non-zero radial electric field at all radii other than r = 0. Virtually all cell designs to date have been crafted such that excitation field or detection field have been optimized, or a compromise has been made between the two. The ability to correct for non-ideal electric fields present during excitation and minimize radial field variation during detection has not been demonstrated with any cell technology. As we and others have shown, radial fields hinder the performance achievable by causing ion dephasing to occur more rapidly. Simulations indicate eTREC technology permits ion excitation to uniform, unstratified cyclotron orbit without z-axis ejection. In addition, the ability to moderate ion dephasing by minimizing radial field variation tunable to any cyclotron radius is maintained. The combination of methods increases instrument performance, since excite coupling provides a more accurately defined cyclotron radius, while minimization of radial fields is tuned for that specific radius. Many benefits result from the eTREC technique, such as improved S/N, limit of detection (LOD), resolution, and sensitivity.

Here we present a novel method of excitation coupling to a modified closed cylindrical cell. Through the use of printed circuit boards for end-cap electrodes, one can produce trapping electrodes with specified geometries to a high degree of precision for a relatively low cost. In addition,

minimization of design complexity can also be achieved with printed circuit board-based design. A capacitive RF voltage divider provides the basis for the RF voltage gradient in this excite-coupled Trapping Ring Electrode Cell (eTREC).

Experimental:

eTREC Design

The conceptual illustration and schematic for the eTREC design was rendered using SolidWorks 2004 (SolidWorks Corp., Suresnes, France). The trap plates were designed in a circuit board layout program EAGLE ver. 4.13 (CadSoft Computer, Pembroke Pines, FL). The printing and machining of the boards was performed by Advanced Circuits (Advanced Circuits, Aurora, CO). The material chosen was FR-4. Out-gassing of the FR-4 circuit board was tested through the addition of a 4" x 8" rectangular multi-layered sheet of this material to the UHV cross and monitoring the achievable base pressure of the high vacuum region. No discernable change in background pressure was observed and others have used this material operating under UHV with minimal out-gassing[32]. The eTREC plates consist of 10 rings per plate (20 independently controlled DC ring potentials total) spaced by a 0.007" gap with a width of 0.066". Tolerances on these dimensions are $\pm$ 0.002". Nine of the ten rings are segmented radially (with the exception of the innermost ring to prevent charging of non-conductor surfaces) again to form four quadrants (90^{o} extent) to which two opposing segments have excitation coupled and adjacent segments have only DC applied. The excitation coupling was performed through a capacitive voltage divider using 680 pF surface mount capacitors (Digikey, Thief River Falls, MN). The RF voltage applied to each ring arc segment beginning from largest radius to smallest radius has about a 10 % $V_{p\text{-}p}$ drop between each arc. This RF voltage drop occurs at each ring arc segment until the center ring is reached which it is then terminated to ground allowing little to no RF onto this ring, effectively making it a DC only ring. The center ring is through hole plated to prevent charging of exposed fiberglass-epoxy composite. RF excitation was prevented from coupling to DC only quadrants via 1 $\mathrm{M}\Omega$ resistors (Digikey,

Thief River Falls, MN) while allowing DC potentials to be coupled to entire rings. Time constants for the switching of DC potentials with all components in place were ~50-100 μs. All components were soldered to the face of the plate external to the trap. Aluminum 2-56 socket cap screws were used to assemble the cell (Fastener Express, Laguna Hills, CA). All twenty rings were wired separately, affording independent control over the DC potentials on each ring. Kapton coated wire (MDC Vacuum Products Corp., Hayward, CA) was used for electrical connections to the trapping ring electrodes. Tin-coated copper ring-tongue solderless connectors (McMaster-Carr, Los Angeles, CA) were used to connect the Kapton wire to the terminals on the cell. The cell had an inner diameter of 1.875" and a length of 2" between trapping electrodes.

eTREC Operation

Generation of independently variable DC voltages for each of the ring electrodes was accomplished using a program developed in-house within LabVIEW 8.0. The process occurs through two computers working in concert, a MIDAS[33] data station and a computer housing the National Instruments hardware. eTREC operation is identical to TREC with two exceptions: the first exception is a solid state relay wired in series with the cylindrical excitation electrodes and the respective trap plate quadrant allows for switching between excite-coupled and uncoupled states using TTL. This arrangement allows for common, TREC, excite-coupled common (ecommon), and eTREC conditions to be accessible to the user without breaking the vacuum or rewiring. The original LabVIEW program was modified to include 10 additional DC potentials to supply the added ring electrodes in the eTREC design.

SIMION Modeling

Modeling of eTREC was performed using SIMION 3D version 7.0 (D. A. Dahl, Idaho National Engineering and Environmental Laboratory). The model was designed to scale with the actual TREC design using 0.25 mm/grid unit and refined to a convergence level of 10^{-5}. Equipotential contour plots illustrate the approximate potentials within the cell during experiments with common voltages, TREC,

ecommon, and eTREC conditions. RF excitation electric field equipotential contours were generated by placing DC potentials of opposite polarity and magnitude reflected about the z-y plane of the cell. The axial and radial field component was recorded and averaged over the entire volume of the cell by acquiring data incrementing cyclotron radius (r = 0, 5, 10, 15, 20 mm) and translating along the z axis (z = 0, 2, 4, 6,…, 50 mm). No TREC (or eTREC) voltage profile was applied during these experiments because voltages during TREC/eTREC experiments are modulated post-excitation.

The extent to which z-axis ejection occurred in each cell was also studied with the SIMION models. A closed cylindrical cell with identical dimensions and aspect ratio was constructed. The user program from the ICR simulation included with SIMION was adapted and used for excitation in both the eTREC and the closed uncoupled cylindrical cell. The starting position of a 1,000 *m/z* ion (zero rest energy) was incremented along the z-axis in order to accurately define the beginning potential energy of the ions. An excitation potential was applied to excite the ions to a final cyclotron radius of 50% of the cell radius. The z component of the velocity (V_z) was recorded. This experiment was repeated with the excitation turned off in both cells. The quantity ΔV_z was calculated by taking the difference in V_z recorded at the center between excitation on and off. The design of this simulation allowed us to show of the change in V_z as a function of z-axis starting position.

FT-ICR MS Experimental Conditions

The spectra presented here were obtained from a constructed-in-house 3.0 T FTICR mass spectrometer. This novel instrument has been described in detail in a recent publication[34].

Radial dependence of signal intensity and S/N ratio of detected FT-ICR signals were investigated with single frequency excitation of bradykinin $[M+2H]^{2+}$ ions. RIPT was used to transfer ion populations to the cell. A frequency of 87.4 kHz was applied for a total of 150 μs to induce coherent cyclotron motion of the ions. 64 K datapoints were collected at 160 kHz. For the investigation of radial dependence on the signal intensity, the following voltage profile was applied to the trapping rings

during detection for both eTREC and TREC: -0.2, 0, 0.3, 0.8, 1.2, 1.6, 1.8, 2.4, 2.8, 3.2 V DC (all experiments). Ion accumulation was set to 250 ms. Excitation was applied for 150 μs duration and amplitude was varied in 3.0 V_{p-p} increments.

The sensitivity experiment was conducted on a set of bradykinin samples with concentrations 10 nM, 50 nM, 100nM, 300 nM, 500 nm, and 1μM. For each cell configuration the excite parameters were tuned independently to yield the most intense ion signal for the bradykinin $[M+2H]^{2+}$ over the data acquisition (64k datapoints @ 160 kHz/s) using 100 nM bradykinin. The ion accumulation time was set to 200 ms. In order to minimize sample carryover and insure accuracy for the sensitivity determination, ESI solution (blank) was run in between successive bradykinin dilutions and 1000 spectra were summed to reveal if any carry over was present. This was repeated until no visible ion signal was detected for bradykinin $[M+2H]^{2+}$. In addition, samples were measured in order of lowest concentration to highest concentration. Since there was no need for hardware modification when switching cell states, data was acquired for all four cell states at each respective concentration without interruption or hardware modification.

The fine structure resolution data was obtained on the peptide MMMMG synthesized in-house. This peptide was purified by preparative reverse phase chromatography prior to mass spectrometric analysis. In this experiment the instrument was set to accumulate ions for 200 ms. A chirp based excitation was used over the frequency range of 20 kHz to 250 kHz. The sweep rate was set to 360 Hz/μs and the amplitude was adjusted for maximum performance of the cell condition in use (eTREC or common (ex) 1.2 V). The 2 M datapoints were acquired at 160 kHz. This resulted in an overall time domain signal length of 6.55 s. Five single scan spectra were recorded in series. The five datasets were internally calibrated using the third isotope peak in the isotopic envelope of MMMMG.

All acquired FT-ICR data were analyzed with ICR-2LS[36]. In all data presented no zero-filling or apodization was performed on the acquired data, with the exception of high resolution MMMMG

spectra. In this case, Welch apodization was applied to the dataset followed by a single zero-fill. Theoretical spectra of MMMMG were generated with the Mercury component[37] in ICR-2LS.

Results

Previous studies of both EPIC and TREC demonstrated increased FTICR-MS performance[13, 25, 26]. With EPIC the cyclotron frequency and observable signal duration was very sensitive to the number of electrons in the electron beam. This initial observation of increased performance when effectively applying a negative potential in the center of the cell, provided the impetus to develop TREC, a cell which allowed us to explore the effects of modulating radial electric fields during detection. In EPIC and TREC the performance enhancement which was observed is directly related to decreasing the variation in radial electric fields during detection. The first generation TREC provided proof of principal in regard to the latter, however, the excitation fields in this cell are non-ideal and lead to z-axis excitation and ion ejection. The non-ideal excitation field has been addressed with the eTREC design while preserving the ability to modulate radial trapping fields during ion detection.

The eTREC design is shown in Figures 2.1A-C. For a detailed description of eTREC see the Methods section. SIMION modeling prior to implementation of eTREC aided in the determination of the most appropriate values for the capacitive voltage divider used. Multiple iterations of applied RF voltage to each arc segment was performed while minimizing the measured axial field to achieve an approximately linear excite field in the RF coupled model. See Supplemental Material for a comparison of the eTREC electrode geometry in an uncoupled vs. a coupled state.

The z-axis ejection of ions during excitation is an observed limitation in the sensitivity of the closed cylindrical cell geometry. This limitation is considered most problematic during modern operation of FT-ICR instruments in which no collisional cooling or adiabatic lowering of trap potentials is utilized to control the kinetic energy of the ions in the cell. The ion population trapped in an actual experiment is likely to contain a broad distribution of energies, and thus, axial amplitudes. Z-axis

A)

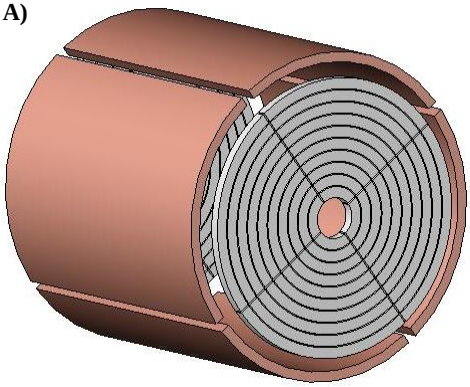

B)

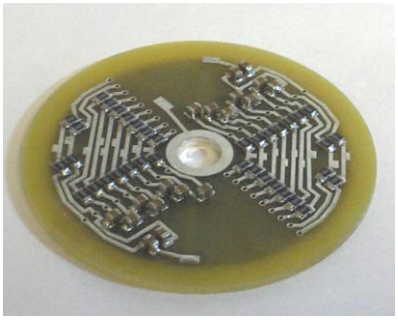

C)

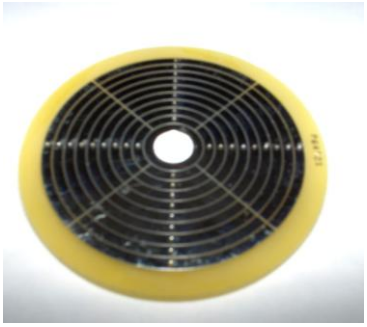

Figure 2.1: A) A conceptual representation of the eTREC design. B) A photograph of the backside of the eTREC trap plate including installed resistor and capacitor components. C) A photograph of the front side of the eTREC trap plate revealing the conductor pattern for the rings and quadrants.

ejection is dependent upon the energy and position of an ion during the excitation. These quantities dictate whether or not the ion remains trapped within the cell subsequent to the excitation event. In order to demonstrate that the eTREC design mitigates this known problem, a simulation of single ion excitation was performed (Figure 2.2). The excitation amplitude was held constant (Vp-p to achieve 50% cell radius) while initial z-axis displacement was incremented from 0 displacement to the boundary of the cell. The change in z-component of the velocity (ΔV_z) was calculated by recording V_z with and without excitation at each z displacement and taking the difference between the two values. A steady increase in the ΔV_z was observed in the uncoupled cell as a function of starting z-axis oscillation amplitude. Eventually, the energy imparted to the ion during the excitation event was enough to overcome the potential well imposed by the trapping electrodes (1.0 V DC). The dashed lines superimposed upon the plot represent the onset of the observation of z-axis ejection at a particular ΔV_z and z-axis displacement in this SIMION model. In the case of eTREC, the trapping ring electrodes were all set to 1.0 V DC to establish the same potential well within both traps. Ideal excitation potentials should induce no increase in the ΔV_z. The eTREC model performed such that z-axis ejection never occurred, even when the ion had z-axis displacement of 99% the cell length. This represents significant improvement over the closed cylindrical

cell. However, eTREC did exhibit deviation from ideal behavior at z-axis displacement >50% cell length. This indicates that the eTREC excitation electrode geometry requires further refinement to achieve a maximum gain in sensitivity. The relative ease in design and fabrication of these trap plates permits further experimentation. SIMION modeling results show qualitative support for the excitation linearization and mitigation of z-axis ejection achieved by the eTREC technology experimentally.

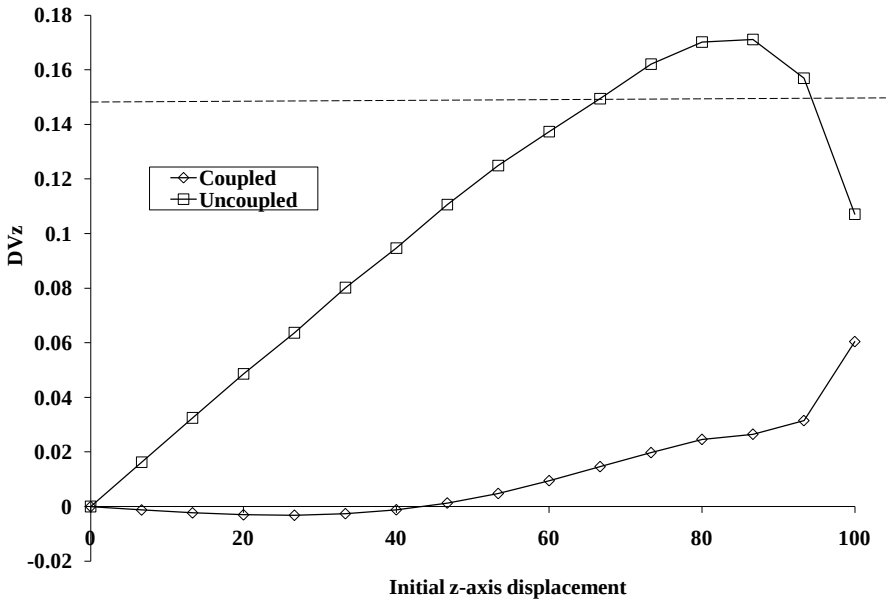

Figure 2.2: SIMION modeling data of velocity increase as a function of initial z-axis displacement. The dashed horizontal line represents the onset of the observation of z-axis ejection in this model.

The sensitivity of the detection process is of great importance in FT based mass analyzers, especially with the present popularity in RF ion trap-FT coupled instruments (LTQ-FT or LTQ-Orbitrap[41]) where the ion trap capacity is generally lower than that of the ICR or Orbitrap mass analyzers. Evaluation of the sensitivity of the four accessible cell configurations (common, TREC, common (ex), and eTREC) was carried out via a serial dilution experiment using Bradykinin $[M+2H]^{2+}$ as the analyte. The percent gain in sensitivity has been quantified as a function of concentration in Figure 2.3. These data were generated by recording the signal amplitude of the first "beat" of Bradykinin $[M+2H]^{2+}$ in each time domain signal and averaging over technical triplicates. This method of recording the intensity of the first "beat" of the time domain signal allows one to minimize effects on the ion intensity which transpire over relatively longer time

periods such as ion cloud dephasing. Therefore, differences in ion intensity must be attributed to z-axis ejection or proximity of the ion cloud to the detection electrodes. The ratio of both eTREC/TREC and common 1.2 V (ex)/common 1.2 V conditions are displayed. The latter two comparisons have been made in order to isolate the sensitivity gain achieved simply through the use of our excitation coupling geometry. The error bars represent $\pm\sigma$. These data indicate >50% gain in sensitivity is achieved when excitation is enabled in both cell operation conditions (TREC or common 1.2 V). This direct experimental observation supports the observations made *in silico* using SIMION modeling which indicate that eTREC operation mitigates z-axis ejection.

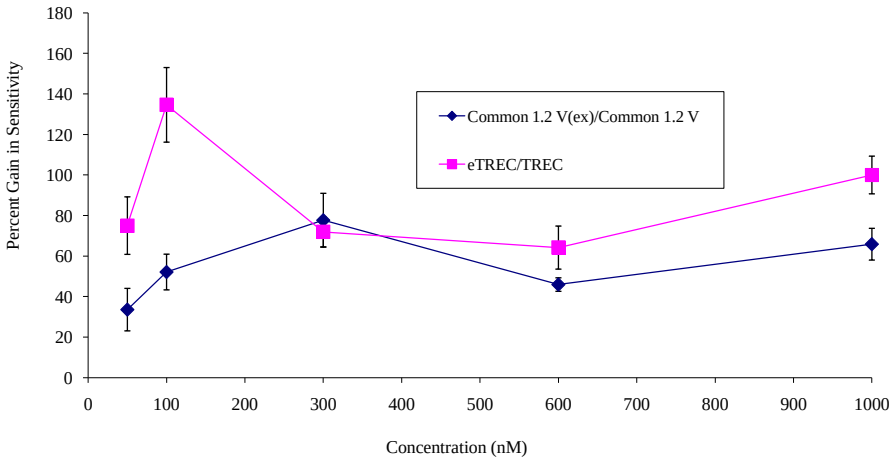

Figure 2.3: The percent gain in sensitivity calculated from the ratio of the first beat intensity for both eTREC/TREC and common (ex) 1.2 V/common 1.2 V cell conditions as a function of concentration. Greater than 50% gain in sensitivity is observed through the use of the excite coupling geometry of this cell.

The resolution achieved by the eTREC technology was demonstrated through the mass measurement of the peptide MMMMG. The third isotope peak in the isotopic envelope contains several possible elemental compositions, the two most abundant are $^{12}C_{22}H_{41}N_5O_6{}^{32}S_3{}^{34}S_1$ and $^{12}C_{20}{}^{13}C_2H_{41}N_5O_6{}^{32}S_4$. The difference in mass between these two species is 10.9 mDa. In order to achieve baseline resolution of these ions, a resolving power of ~200,000 is required. Figure 2.4 shows data acquired under eTREC conditions. The ability to resolve fine structure at modest magnetic field strength has been shown by others[42]; however, prior examples involve adiabatic ramping of trapping

potentials, minimization of ion population, collisional cooling, and other adjustments for minimization of the probability that these two distinct masses will be observed as a single mass. In the case of eTREC none of these methods were utilized, which indicates that minimization of the radial field environment

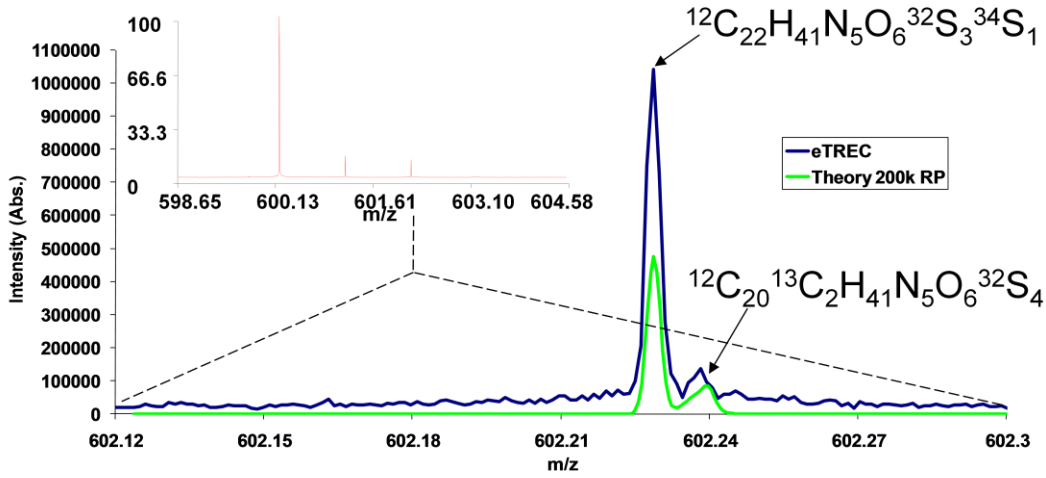

Figure 2.4: Five consecutively acquired single scans of MMMMG peptide $[M+H]^+$ internally calibrated and summed. The mass range in view is centered about the 3rd isotope peak in the envelope using eTREC.

in the cell allows not only higher resolving power, but greater resolution. These data illustrate the fundamental difference between resolving power and resolution. In the previous report it was shown that TREC technology increases phase coherence of ions and allows for observation of coherent ion motion for longer time periods; the observed frequency drift over long acquisition periods was also shown to be minimized as well. Minimization of the drift in frequency over the acquisition period is likely accountable for the increased resolution observed with eTREC. However, another possibility is that eTREC conditions reduce the probability of coalescence between two closely space m/z species, although no experiment data is provided to support this. The ability to simultaneously detect very closely spaced molecular species is important for improving the depth of information[43] obtained from analysis in all fields which utilize high resolution mass spectrometry. In proteomics, isobaric amino acid

substitutions (Met + Leu versus Pro + Phe) and peptide modifications (phosphorylation versus sulfation) exist in which the mass difference to be resolved is of the same order of magnitude[44].

Conclusions:

The eTREC technology provides an efficient method for linearization of excitation fields. This first generation example of eTREC allowed for a >50% gain in sensitivity and a lower LOD, which has been primarily attributed to mitigation of z-axis ejection during ion excitation. The ability to manipulate the radial field environment within the cell was shown to be retained within this design, giving it the same increased detection performance as its predecessor, TREC. Fine structure resolution of the peptide MMMMG was observed using the eTREC technology at modest magnetic field strength, while using common (ex) 1.2 V conditions fine structure was not observed althoughRP~300000 was achieved for both cell states. Direct experimental observation supports SIMION modeling results performed during conception of eTREC. However, deviation from excitation field ideality in close proximity to the trapping electrodes leaves room for improvement in the present design of eTREC. As a first generation design, eTREC has provided a straight forward and efficient vehicle toward proof of principal for this technology.

Acknowledgements

The authors acknowledge Alan Marshall and his group at the National High Magnetic Field Laboratory for the use of the MIDAS data station. We would also like to thank Gordon Anderson for helpful discussion on implementation of electronics for eTREC. This material is based upon work supported by the Directorate of Biological Sciences, National Science Foundation under Grant No. 0352451; Murdock Charitable Trust; and Office of Science (BER), U.S. Department of Energy, Grant No. DE-FG02-04ER63924.

Bibliography

(1) Comisarow, M. B.; Marshall, A. G. *Chemical Physics Letters* 1974, *25*, 282-283.

(2) He, F.; Emmett, M. R.; Hakansson, K.; Hendrickson, C. L.; Marshall, A. G. *J. Proteome Res.* 2004, *3*, 61-67.

(3) Gabrielse, G.; Haarsma, L.; Rolston, S. L. *International Journal of Mass Spectrometry and Ion Processes* 1989, *88*, 319-332.

(4) Williams, D. K.; Hawkridge, A. M.; Muddiman, D. C. *Journal of the American Society for Mass Spectrometry* 2007, *18*, 1-7.

(5) Wong, R. L.; Amster, I. J. *Journal of the American Society for Mass Spectrometry* 2006, *17*, 1681-1691.

(6) Schmidt, A.; Gehlenborg, N.; Bodenmiller, B.; Mueller, L. N.; Campbell, D.; Mueller, M.; Aebersold, R.; Domon, B. *Mol Cell Proteomics* 2008, *7*, 2138-2150.

(7) Rinner, O.; Seebacher, J.; Walzthoeni, T.; Mueller, L. N.; Beck, M.; Schmidt, A.; Mueller, M.; Aebersold, R. *Nat Methods* 2008, *5*, 315-318.

(8) Brown, S. C.; Kruppa, G.; Dasseux, J.-L. *Mass Spectrometry Reviews* 2005, *24*, 223-231.

(9) Han, J.; Danell, R. M.; Patel, J. R.; Gumerov, D. R.; Scarlett, C. O.; Speir, J. P.; Parker, C. E.; Rusyn, I.; Zeisel, S.; Borchers, C. H. *Metabolomics* 2008, *4*, 128-140.

(10) Rodgers, R. P.; Schaub, T. M.; Marshall, A. G. *Analytical Chemistry* 2005, *77*, 20A-27A.

(11) Marshall, A. G.; Rodgers, R. P. *Accounts of Chemical Research* 2004, *37*, 53-59.

(12) Kaiser, N. K.; Skulason, G. E.; Weisbrod, C. R.; Wu, S.; Zhang, K.; Prior, D. C.; Buschbach, M. A.; Anderson, G. A.; Bruce, J. E. *Rapid Commun Mass Spectrom* 2008, *22*, 1955-1964.

(13) Weisbrod, C. R.; Kaiser, N. K.; Skulason, G. E.; Bruce, J. E. *Anal Chem* 2008, *80*, 6545-6553.

(14) Beu, S. C.; Laude, D. A., Jr. *Analytical Chemistry* 1992, *64*, 177-180.

(15) Bruce, J. E.; Anderson, G. A.; Lin, C.-Y.; Gorshkov, M.; Rockwood, A. L.; Smith, R. D. *Journal of Mass Spectrometry* 2000, *35*, 85-94.

(16) Brustkern, A. M.; Rempel Don, L.; Gross Michael, L., Indianapolis, IN 2007.

(17) Caravatti, P.; Allemann, M. *Organic Mass Spectrometry* 1991, *26*, 514-518.

(18) Gabrielse, G.; MacKintosh, F. C. *International Journal of Mass Spectrometry and Ion Processes* 1984, *57*, 1-17.

(19) Vartanian, V. H.; Hadjarab, F.; Laude, D. A. *International Journal of Mass Spectrometry and Ion Processes* 1995, *151*, 175-187.

(20) Wang, M.; Marshall, A. G. *Analytical Chemistry* 1989, *61*, 1288-1293.

(21) Yin, W. W.; Wang, M.; Marshall, A. G.; Ledford, E. B., Jr. *Journal of the American Society for Mass Spectrometry* 1992, *3*, 188-197.

(22) Guan, S.; Marshall, A. G. *International Journal of Mass Spectrometry and Ion Processes* 1995, *146/147*, 261-296.

(23) Marshall, A. G.; Hendrickson, C. L.; Jackson, G. S. *Mass Spectrometry Reviews* 1998, *17*, 1-35.

(24) Kaiser, N. K.; Weisbrod, C. R.; Webb, B. N.; Bruce, J. E. *Journal of the American Society for Mass Spectrometry* 2008, *19*, 467-478.

(25) Kaiser, N. K.; Bruce, J. E. *International Journal of Mass Spectrometry* 2007, *265*, 271-280.

(26) Kaiser, N. K.; Bruce, J. E. *Analytical Chemistry* 2005, *77*, 5973-5981.

(27) Kim, S.; Choi, M. C.; Kim, S.; Hur, M.; Kim, H. S.; Yoo, J. S.; Blakney, G. T.; Hendrickson, C. L.; Marshall, A. G. *Analytical Chemistry* 2007, *79*, 3575-3580.

(28) Mitchell, D. W.; Hearn, B. A.; DeLong, S. E. *International Journal of Mass Spectrometry and Ion Processes* 1993, *125*, 95-126.

(29) Wang, M.; Marshall, A. G. *Analytical Chemistry* 1990, *62*, 515-520.

(30) Van der Hart, W. J.; Van de Guchte, W. J. *International Journal of Mass Spectrometry and Ion Processes* 1988, *82*, 17-31.

(31) Tolmachev, A. V.; Robinson, E. W.; Wu, S.; Kang, H.; Lourette, N. M.; Pasa-Tolic, L.; Smith, R. D. *Journal of the American Society for Mass Spectrometry* 2008, *19*, 586-597.

(32) Rouki, C.; Westerberg, L. *Physica Scripta, T* 2003, *T104*, 107-108.

(33) Senko, M. W.; Canterbury, J. D.; Guan, S.; Marshall, A. G. *Rapid Communications in Mass Spectrometry* 1996, *10*, 1839-1844.

(34) Kaiser, N. K.; Skulason, G. E.; Weisbrod, C. R.; Bruce, J. E. *J Am Soc Mass Spectrom* 2009, *20*, 755-762.

(35) Wu, S.; Zhang, K.; Kaiser, N. K.; Bruce, J. E.; Prior, D. C.; Anderson, G. A. *Journal of the American Society for Mass Spectrometry* 2006, *17*, 772-779.

(36) Anderson, G. A.; Bruce, J. E.; Smith, R. D., 2.18 ed.: Richland, WA, 1996.

(37) Rockwood, A. L. *Rapid Communications in Mass Spectrometry* 1995, *9*, 103-105.

(38) Wu, S.; Lourette, N. M.; Tolic, N.; Zhao, R.; Robinson, E. W.; Tolmachev, A. V.; Smith, R. D.; Pasa-Tolic, L. *Journal of Proteome Research* 2009, *8*, 1347-1357.

(39) Kelleher, N. L. *Anal Chem* 2004, *76*, 197A-203A.

(40) Kelleher, N. L.; Nicewonger, R. B.; Begley, T. P.; McLafferty, F. W. *J. Biol. Chem.* 1997, *272*, 32215-32220.

(41) Makarov, A.; Denisov, E.; Kholomeev, A.; Balschun, W.; Lange, O.; Strupat, K.; Horning, S. *Anal Chem* 2006, *78*, 2113-2120.

(42) Solouki, T.; Emmett, M. R.; Guan, S.; Marshall, A. G. *Analytical Chemistry* 1997, *69*, 1163-1168.

(43) Spengler, B. *Journal of the American Society for Mass Spectrometry* 2004, *15*, 703-714.

(44) Bossio, R. E.; Marshall, A. G. *Analytical chemistry* 2002, *74*, 1674-1679.